



Climate change increases riverine carbon outgassing, while export to the ocean remains uncertain

F. Langerwisch^{1,2}, A. Walz³, A. Rammig^{1,4}, B. Tietjen^{5,2}, K. Thonicke^{1,2}, and W. Cramer^{6,2}

¹Earth System Analysis, Potsdam Institute for Climate Impact Research (PIK), P.O. Box 601203, Telegraphenberg A62, 14412 Potsdam, Germany

²Berlin-Brandenburg Institute of Advanced Biodiversity Research (BBIB), 14195 Berlin, Germany

³Institute of Earth and Environmental Science, University of Potsdam, Karl-Liebknecht-Str. 24–25, 14476 Potsdam-Golm, Germany

⁴TUM School of Life Sciences Weihenstephan, Land Surface-Atmosphere Interactions, Technical University Munich, Hans-Carl-von-Carlowitz-Platz 2, 85354 Freising, Germany

⁵Biodiversity – Ecological Modelling, Institute of Biology, Freie Universität Berlin, Altensteinstr. 6, 14195 Berlin, Germany

⁶Institut Méditerranéen de Biodiversité et d'Ecologie marine et continentale (IMBE), Aix-Marseille Université, CNRS, IRD, Avignon Université, Technopôle Arbois-Méditerranée, Bât. Villemain – BP 80, 13545 Aix-en-Provence CEDEX 04, France

Correspondence to: F. Langerwisch (langerwisch@pik-potsdam.de)

Received: 25 June 2015 – Published in Earth Syst. Dynam. Discuss.: 17 August 2015

Revised: 19 March 2016 – Accepted: 13 June 2016 – Published: 8 July 2016

Abstract. Any regular interaction of land and river during flooding affects carbon pools within the terrestrial system, riverine carbon and carbon exported from the system. In the Amazon basin carbon fluxes are considerably influenced by annual flooding, during which terrigenous organic material is imported to the river. The Amazon basin therefore represents an excellent example of a tightly coupled terrestrial–riverine system. The processes of generation, conversion and transport of organic carbon in such a coupled terrigenous–riverine system strongly interact and are climate-sensitive, yet their functioning is rarely considered in Earth system models and their response to climate change is still largely unknown. To quantify regional and global carbon budgets and climate change effects on carbon pools and carbon fluxes, it is important to account for the coupling between the land, the river, the ocean and the atmosphere. We developed the RIVERine Carbon Model (RivCM), which is directly coupled to the well-established dynamic vegetation and hydrology model LPJmL, in order to account for this large-scale coupling. We evaluate RivCM with observational data and show that some of the values are reproduced quite well by the model, while we see large deviations for other variables. This is mainly caused by some simplifications we assumed. Our evaluation shows that it is possible to reproduce large-scale carbon transport across a river system but that this involves large uncertainties. Acknowledging these uncertainties, we estimate the potential changes in riverine carbon by applying RivCM for climate forcing from five climate models and three CO₂ emission scenarios (Special Report on Emissions Scenarios, SRES). We find that climate change causes a doubling of riverine organic carbon in the southern and western basin while reducing it by 20 % in the eastern and northern parts. In contrast, the amount of riverine inorganic carbon shows a 2- to 3-fold increase in the entire basin, independent of the SRES scenario. The export of carbon to the atmosphere increases as well, with an average of about 30 %. In contrast, changes in future export of organic carbon to the Atlantic Ocean depend on the SRES scenario and are projected to either decrease by about 8.9 % (SRES A1B) or increase by about 9.1 % (SRES A2). Such changes in the terrigenous–riverine system could have local and regional impacts on the carbon budget of the whole Amazon basin and parts of the Atlantic Ocean. Changes in riverine carbon could lead to a shift in the riverine nutrient supply and pH, while changes in the exported carbon

to the ocean lead to changes in the supply of organic material that acts as a food source in the Atlantic. On larger scales the increased outgassing of CO₂ could turn the Amazon basin from a sink of carbon to a considerable source. Therefore, we propose that the coupling of terrestrial and riverine carbon budgets should be included in subsequent analysis of the future regional carbon budget.

1 Introduction

Research on the effects of climate and land use change on terrestrial and riverine systems has been extensively conducted. Results show how changes in temperature and precipitation will affect the species composition in forest ecosystems (Fearnside, 2004; Huntingford et al., 2013; Nepstad et al., 2007) as well as discharge and flooding patterns of rivers (Coe et al., 2011; Panday et al., 2015; Zulkafli et al., 2016). However, the consequences for a coupled terrestrial–riverine system have been elaborated on in less detail, mostly focusing on estimations under the current climate (Johnson et al., 2006; Cole et al., 2000; Richey et al., 2002; Neu et al., 2011; Abril et al., 2014). Here we want to deepen the understanding of consequences of climate change on riverine carbon fluxes, which are fuelled by vegetation, and on the export of carbon from the terrestrial part to the atmosphere and the ocean. We aim to understand how much the basin-wide carbon balance is influenced by these interactions.

In this study we focus on the coupled terrestrial–riverine system in the Amazon basin. In this region the Amazon River and, in particular, the annually recurring flooding of parts of the forests shape the manifold Amazonian ecosystems. The flooding is most decisive for the coupling of terrestrial and aquatic processes by transferring organic material from the terrestrial ecosystems to the river (Hedges et al., 2000). The water rises with an amplitude of only some centimetres in small tributaries to up to 15 m in the main stem (Junk, 1985). In central Amazonia about 16 % of the area is flooded during high water, while only 4 % is flooded permanently (Richey et al., 2002). During flooding, deposited litter and soil carbon which originates from terrestrial vegetation is one source of organic material imported into the river system. The input of terrigenous organic material affects the riverine system enormously on a local scale (Melack and Forsberg, 2001; Waterloo et al., 2006). It acts, for instance, as fertilizer and food source (Anderson et al., 2011; Horn et al., 2011) and is a modifier of habitats and interacting local carbon cycles (Hedges et al., 2000; Irmiler, 1982; Johnson et al., 2006; McClain and Elsenbeer, 2001). Whereas in most limnic systems additional organic material produced by aquatic photosynthesis plays a major role for the riverine organic carbon pools (Lampert and Sommer, 1999; Schwoerbel and Brendelberger, 2005), the aquatic photosynthesis rate in large parts of the Amazon River network is comparably low and submerged plants rarely occur (Junk and Piedade, 1997). Here, the input of allochthonous material produced

in the floodplain forests is more relevant than the production of organic matter within the river (Abril et al., 2014; Cole and Caraco, 2001; Druffel et al., 2005; Mayorga et al., 2005). The low aquatic productivity in the river system is caused by a high sediment load and thus high turbidity in white-water rivers and a low nutrient supply in the black-water rivers (Benner et al., 1995; Richey et al., 1990; Sioli, 1957).

On larger scales, the release of carbon into the atmosphere and the export to the ocean are the most relevant factors, when it comes to estimating the effects of Amazon ecosystems on climate change. Approximately $32.7 \times 10^{12} \text{ g C yr}^{-1}$ (Moreira-Turcq et al., 2003) of total organic carbon (TOC) is exported to the Atlantic Ocean, in comparison to about $470 \times 10^{12} \text{ g C yr}^{-1}$ (Richey et al., 2002) exported to the atmosphere as CO₂. While the carbon released to the atmosphere proliferates climate change immediately, the carbon exported to the ocean affects the marine ecosystems over hundreds of square kilometres off the mouth of the Amazon River, thereby possibly influencing ocean–atmosphere carbon exchange over several weeks to months (Cooley et al., 2007; Cooley and Yager, 2006; Körtzinger, 2003; Subramaniam et al., 2008).

The hydrologic or limnic production as well as the transformation and export of carbon have been estimated in a number of empirical (case) studies. These studies highlight different aspects of the system, e.g. showing that the carbon within the river mainly originates from tree leaves and other non-woody material from *várzea* systems (Hedges et al., 2000; Moreira-Turcq et al., 2003), describing reasons for temporal and spatial differentiations of organic matter within the river (Aufdenkampe et al., 2007; Devol et al., 1995), and modelling the hydrological and biochemical aquatic carbon budget over a 2000 km reach (Bustillo et al., 2011). Several studies already combined the aquatic and the terrestrial compartment of the system by including the adjacent forests (Johnson et al., 2006; Cole et al., 2000; Richey et al., 2002; Neu et al., 2011; Abril et al., 2014), but these studies focus on estimating carbon budgets under current climate conditions.

By improving the understanding of how future climate change could influence the largest interconnected ecosystem on Earth (Bauer et al., 2013; Sjögersten et al., 2014), an in-depth analysis of the coupled terrigenous–riverine carbon fluxes and pools in the Amazon basin is required. Climate and atmospheric CO₂, terrestrial productivity, water discharge and flooding patterns strongly interact and thus control the amount of carbon in the Amazon River. But they

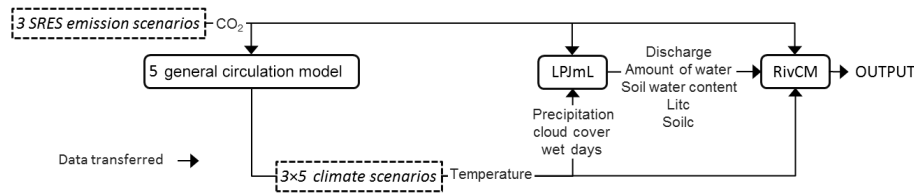


Figure 1. Overview of the transfer of data between the models and scenarios.

also influence its further conversion and transport within the river system, which finally determine carbon export to either atmosphere or ocean. This tight coupling of the terrigenous–riverine system makes the Amazon basin highly sensitive to climate change impacts.

This study aims at taking first steps towards an understanding of carbon fluxes in a terrigenous river–ocean system under future climate change by addressing the following research questions for the example of the Amazon basin:

1. How will the highly interdependent and strongly climate-controlled carbon fluxes and pools in the Amazon basin change during the 21st century?
2. Which regions in the Amazon basin are likely to be most strongly impacted by climate change?
3. How does climate change alter the proportion of carbon immediately released to the atmosphere vs. carbon exported to the ocean?
4. How relevant is the amount of riverine outgassed carbon for the basin-wide carbon budget in a changing climate?

To address these questions we developed the RIVERine Carbon Model (RivCM) and applied it to the Amazon basin. RivCM is directly coupled to the dynamic vegetation and hydrology model LPJmL (Bondeau et al., 2007; Gerten et al., 2004; Rost et al., 2008; Sitch et al., 2003). The riverine carbon model focuses on the export, transport and conversion of terrestrial fixed carbon. Carbon pools and fluxes for the most important transport and transformation processes are validated for current conditions based on observational data from the Amazon basin.

To investigate potential future changes in the different carbon fluxes and pools, the model was forced by climate change scenarios that cover a large range of uncertainty in climate change projections for the Amazon basin. Based on these simulations, we identify areas most heavily affected by climate change. We estimated temporal changes in the different carbon fluxes and pools, as well as the carbon released to the atmosphere and exported to the ocean. To additionally assess the benefit of including inundated areas in the model, a full factorial experiment was conducted. In this way, the study aims to develop a concept to assess changes in coupled terrestrial–riverine systems, which is a prerequisite to better quantify regional and global carbon budgets and consequences of climate change.

2 Methods

RivCM is a grid-based model simulating riverine carbon dynamics on monthly time steps. It is coupled to the process-based dynamic global vegetation and hydrology model LPJmL (Bondeau et al., 2007; Gerten et al., 2004; Rost et al., 2008; Sitch et al., 2003). RivCM is driven by current and future climate and atmospheric CO₂ data. An overview about the interconnection between the models and scenarios is given in Fig. 1.

2.1 Model descriptions

2.1.1 The dynamic global vegetation and hydrology model LPJmL

The process-based dynamic global vegetation and hydrology model LPJmL (Bondeau et al., 2007; Gerten et al., 2004; Rost et al., 2008; Sitch et al., 2003) calculates carbon and corresponding water fluxes globally with a spatial resolution of $0.5 \times 0.5^\circ$ (lat \times long) and daily time steps. For the simulation of potential natural vegetation and the main processes controlling its dynamics, LPJmL uses climate data (temperature, precipitation and cloud cover), atmospheric CO₂ and soil texture as input. The main processes are photosynthesis based on Farquhar et al. (1980) and Collatz et al. (1992), auto- and heterotrophic respiration, establishment, mortality and phenology. These processes lead to dynamic changes in carbon stored in the vegetation, litter and soil. Simulated water fluxes include evaporation, soil moisture, snowmelt, runoff, discharge, interception and transpiration. Globally, LPJmL calculates the performance of nine plant functional types in each grid cell, each of these representing an assortment of species classified as being functionally similar. In the Amazon basin, LPJmL primarily simulates three of these plant functional types, representing tropical evergreen and deciduous forest and C4 grasses. The monthly aggregated amounts of carbon stored in litter and soil, as well as the grid cell's amount of discharged and stored water are used as an input to RivCM.

LPJmL has been shown to reproduce current patterns of biomass production, river discharge and carbon emission through fire and also includes managed land (Biemans et al., 2009; Bondeau et al., 2007; Cramer et al., 2001; Fader et al., 2010; Gerten et al., 2004, 2008; Poulter et al., 2009a; Rost et al., 2008; Sitch et al., 2003; Thonicke et al., 2010; Wagner et

al., 2003). The observed patterns in water fluxes, such as soil moisture, evapotranspiration and runoff, are comparable to stand-alone global hydrological models (Wagner et al., 2003; Gerten et al., 2004, 2008; Gordon et al., 2004; Biemans et al., 2009). Several studies on Amazonia have been conducted showing the effect of climate change on net primary production (NPP; Poulter et al., 2009b), on carbon stocks (Gumpenberger et al., 2010), on the risk for forest dieback (Rammig et al., 2010) and also on riverine-related changes such as inundation patterns (Langerwisch et al., 2013; Zulkafli et al., 2016). The ability of the model to realistically reproduce both terrestrial carbon and water fluxes and pools makes it an excellent tool to investigate the coupling of the terrestrial and riverine carbon in the Amazon basin.

2.1.2 The riverine carbon model RivCM

RivCM is a process-based model which simulates the most important processes impacting different riverine carbon pools, namely import, conversion and export (see overview in Fig. 2). The model calculates the four major ecological processes related to the riverine carbon budget of the Amazon River: mobilization of terrigenous organic material (litter and soil carbon), (mechanical) decomposition of terrigenous organic material, (biochemical) respiration of terrigenous organic material and outgassing of CO_2 to the atmosphere. These processes directly control the most relevant riverine carbon pools, specifically particulate organic carbon (POC), dissolved organic carbon (DOC) and inorganic carbon (IC), as well as outgassed carbon (representing CO_2) and exported riverine carbon to the ocean (POC, DOC and IC). Since RivCM is developed to simulate the fate of terrigenous carbon, it ignores the autochthonous production of organic material within the river. A description of the model including sensitivity analysis and parameterization can be found in the following and in the Supplement.

The Amazon River mobilizes large amounts of terrigenous organic material from seasonally flooded forests (Litc and Soilc in Fig. 2), where dead leaves and twigs are exported to the river (Irmeler, 1982; Wantzen et al., 2008). Given the high productivity in Amazonian forests, this mobilization considerably increases the amount of organic material in the water (Junk, 1985; Cole and Caraco, 2001; Junk and Wantzen, 2004). Johnson et al. (2006) and Cole et al. (2000) showed that terrestrially fixed carbon from the floodplain forests is the major source of respired organic matter within the river and lakes. In RivCM the mobilization process is presented by a function that calculates the amount of mobilized terrestrially fixed carbon in currently inundated areas (POC and DOC in Fig. 2) depending on the amount of available exportable terrestrial organic carbon from dead matter. The monthly inundated area is calculated using current discharge and discharge from the reference period 1971–2000 and potentially floodable area (Langerwisch et al., 2013).

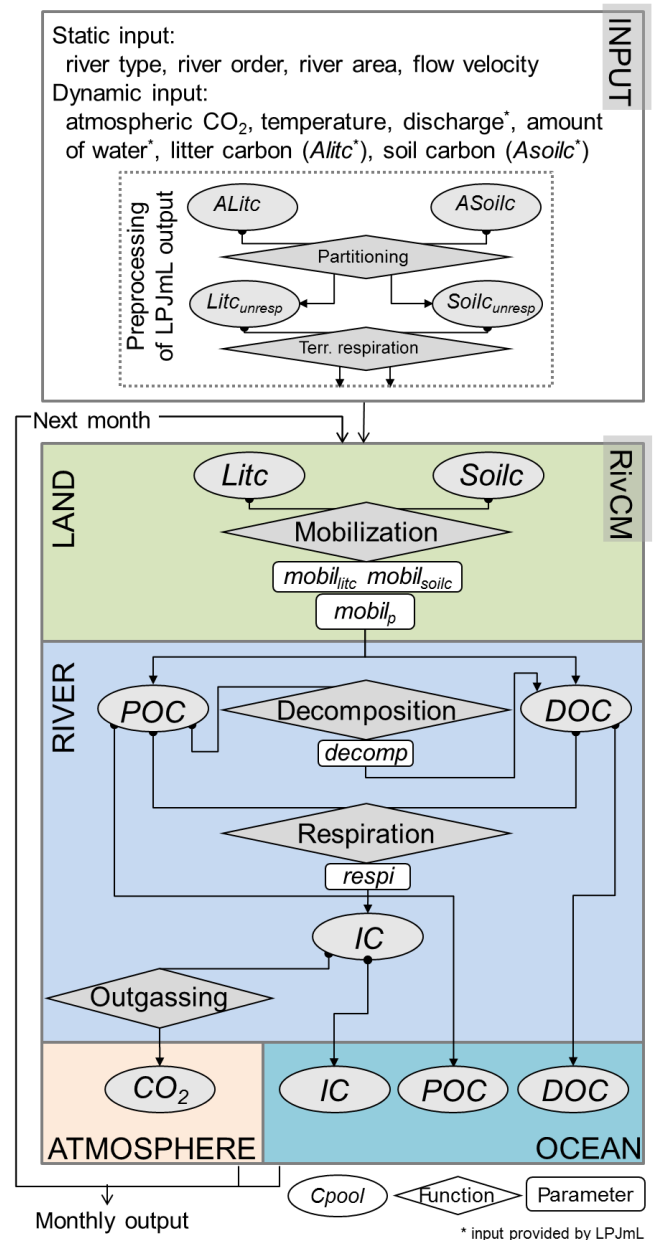


Figure 2. Input and flow chart of RivCM. The four spatial components “LAND”, “RIVER”, “ATMOSPHERE” and “OCEAN” are connected by the exchange of carbon between different carbon pools (ovals). The carbon pools are transformed through the most relevant processes (diamonds) with specific rates and ratios (rectangles). After the initialization of the input, calculations are conducted on a monthly basis. Litc: carbon in litter; Soilc: carbon in soil; POC: particulate organic carbon; DOC: dissolved organic carbon; IC: inorganic carbon.

Besides the import of terrigenous material, another source of organic matter for the river is the allochthonous production. In most limnic systems the production of organic material by photosynthesis by aquatic plants plays a major role

in the organic carbon pool (Lampert and Sommer, 1999; Schwoerbel and Brendelberger, 2005). In Amazonia, however, the aquatic photosynthesis rate in large parts of the Amazon River network is comparably low and submerged plants rarely occur (Junk and Piedade, 1997) since the white-water rivers contain large amounts of sediments and are thus turbid and the black-water rivers contain only little nutrients (Benner et al., 1995; Richey et al., 1990; Sioli, 1957). Therefore, the input of allochthonous material produced in floodplain forests contributes much more strongly to total organic matter within the river than the production by aquatic plants (Cole and Caraco, 2001; Junk, 1985; Junk and Wantzen, 2004). Therefore, the Amazon River itself is considered a transport agent rather than a producer of organic material (Junk and Wantzen, 2004). For these reasons the calculation of riverine primary production, via aquatic photosynthesis, has been omitted in the model calculations.

In the river, the imported organic matter is decomposed by manual breakup by either abiotic decomposition like grinding or by biotic fragmentation by shredders such as Gammaridae or fish (Hedges et al., 1994; Martius, 1997; Melack and Forsberg, 2001). Moreover, decomposition includes the leaching of coarse and fine material to form dissolved organic carbon (DOC in Fig. 2) (Lampert and Sommer, 1999). This enlarges the surface for colonization by fungi and bacteria which are responsible for biochemical decomposition (respiration) (Martius, 1997; Wantzen et al., 2008). During heterotrophic respiration, most of the ingested carbon is released as CO₂ to the water body (IC in Fig. 2).

Outgassing, i.e. the evasion of gases from the water body, occurs, when the concentration of a specific gas in the water body exceeds its saturation concentration which depends on temperature and partial pressure (Schwoerbel and Brendelberger, 2005). Due to a high carbon input into the Amazonian rivers, large amounts of CO₂ and CH₄ are produced and saturate the water (Mayorga et al., 2005; Richey et al., 2002). The outgassing of CO₂ contributes more than 95 % to the total outgassed carbon (Belger et al., 2011; Melack et al., 2004; Richey et al., 2002). We therefore considered only the outgassing of CO₂ in the model (CO₂ in Fig. 2).

An overview of model input, comprising static data (describing fixed site conditions) and dynamic data, like climate, atmospheric CO₂ concentration and terrigenous organic carbon, is given in Table 1. Physical constants are listed in Table 2. The following sections describe the input data, the modelling approach of individual processes and the coupling to LPJmL.

Input data and RivCM model initialization

River type and river order (Fig. 3), as well as river area, which represents about 25 % of the potential floodable area (Langerwisch et al., 2013; Richey et al., 2002), prescribe the size and characteristics of the river stretch. The river type of each cell was defined by combining information published

by Sioli (1957), Irion (1976) and Diegues (1994), and can be either white, black or clear water. The river colour depends on the amount of sediments and dissolved organic material in the water. It determines, amongst other things, the pH and the temperature. For simplification, very small catchments (smaller than the simulated resolution) of deviating river types were ignored and the dominant river type was used. River order is represented by three classes and defined by total annual discharge (headwater: $< 8 \times 10^3 \text{ m}^3 \text{ yr}^{-1}$; middle reach: 8×10^3 to $2 \times 10^5 \text{ m}^3 \text{ yr}^{-1}$; lower reach: $> 2 \times 10^5 \text{ m}^3 \text{ yr}^{-1}$). We chose these classes because of their different characteristics, as discussed in the River Continuum Concept (Vannote et al., 1980). Each grid cell that receives the routed water (rout cell) is determined by a digital elevation model (as also in Rost et al., 2008). The water is routed with a slope-dependent flow velocity v (m s^{-1}) (Langerwisch et al., 2013), which results in a distance of about 13 cells being routed through per month (in the largest part of the basin).

Data input from LPJmL to RivCM

Monthly discharge (Mdis ($\text{m}^3 \text{ s}^{-1}$)), amount of water (Mwat (m^3)) and soil water content for two soil layers (Mswc₁ within the upper soil layer (soildepth₁ = 200 cm) and Mswc₂ within the lower soil layer (soildepth₂ = 300 cm) (%)) are provided by LPJmL. Additionally, annual litter carbon (ALitic (g m^{-2})) and soil carbon (ASoilc (g m^{-2})) are provided by LPJmL (see also Figs. 1 and 2). The coupling is unidirectional. RivCM uses the LPJ output as input, but the processes calculated only affect the carbon pools and fluxes in RivCM. The carbon stored in litter and soil is calculated in LPJmL, while for simplification the reduction in litter due to the mobilization is not fed back to LPJmL.

Atmospheric CO₂ concentration (atmCO₂ (ppm)) and monthly temperature (T (°C)) prescribing abiotic atmospheric conditions are derived from the climate input data sets (see Sect. 2.2).

Water temperature

Water temperature at time t (°C) depends on air temperature $T_{\text{air}t}$ (°C) and river colour, given by river type. In white- and clear-water rivers the temperature is below air temperature. The calculation of the water temperature of these rivers is conducted according to Eq. (1) based on Bogan et al. (2003), with T_t calculated as

$$T_t = 0.6946 \times T_{\text{air}t} + 5.19. \quad (1)$$

The temperature in black-water rivers is close to air temperature.

Temperature response

The respiration reaction calculated in RivCM at time t is adjusted according to the water temperature T_t by a coefficient

Table 1. Overview of the input used in the model.

Input	Temporal resolution	Spatial resolution (lat × long)	Unit	Source
Static				
River type	–	0.5° × 0.5°	–	Diegues (1994); Irion (1976); Sioli (1957)
River order	–	0.5° × 0.5°	–	
Max. floodable area (MaxInunArea)	–	0.5° × 0.5°	km ²	Langerwisch et al. (2013)
Rout cell	–	0.5° × 0.5°	–	Rost et al. (2008)
Flow velocity (<i>v</i>)	–	0.5° × 0.5°	m s ⁻¹	Langerwisch et al. (2013)
Soil depth (soildepth ₁ , soildepth ₂)	–	0.5° × 0.5°	cm	LPJmL
Dynamic				
Atmospheric CO ₂ (atmCO ₂)	Annual	Global	ppm	SRES; see Nakićenović et al. (2000)
Temperature (<i>T</i>)	Monthly	0.5° × 0.5°	° C	IPCC; see Meehl et al. (2007)
Discharge (Mdis)	Monthly	0.5° × 0.5°	m ³ s ⁻¹	LPJmL
Amount of water (Mwat)	Monthly	0.5° × 0.5°	m ³	LPJmL
Soil water content (Mswc ₁ , Mswc ₂)	Monthly	0.5° × 0.5°	%	LPJmL
Soil carbon (ASoile)	Annual	0.5° × 0.5°	g m ⁻²	LPJmL
Litter carbon (ALitc)	Annual	0.5° × 0.5°	g m ⁻²	LPJmL

Table 2. List of physical constants.

Constant name	Value	Unit	Source
k_H^θ	1.496323	g CO ₂ L ⁻¹ atm ⁻¹	Sander (1999)
dlnkH	2400	K	Sander (1999)
T^θ	298.15	K	Sander (1999)
ctoco2*	0.2729	–	

* Ratio of the atomic mass of carbon (12.001 g mol⁻¹) in the CO₂ molecule (44.01 g mol⁻¹). Applied to calculate the outgassed CO₂, since the model calculates the actual flux and pools of carbon.

for temperature response, T_{response_t} (Eq. (2); Lampert and Sommer, 1999). Additionally to the temperature response in water (and water-saturated soil), a temperature response for (unsaturated) soils was calculated with Eq. (3).

$$T_{\text{response}_t} = e^{308.56 \times \left(\frac{1}{56.02} - \frac{1}{T_t + 46.02} \right)} \quad (2)$$

$$T_{\text{response}_{\text{dry}_t}} = T_{\text{response}_t} \times \frac{1 - \left(e^{-\frac{M_{\text{swc}_1} \times \text{soildepth}_1 + M_{\text{swc}_2} \times \text{soildepth}_2}{\text{soildepth}_1 + \text{soildepth}_2}} \right)}{1 - (e^{-1})} \quad (3)$$

This is based on the empirical relationship of temperature response in soils (Lloyd and Taylor (1994) also applied in LPJmL), which is valid for temperatures above -40° C.

Initialization of litter and soil carbon

As initialization for Litc and Soile in the first simulated month, RivCM uses the litter and soil carbon stocks (ALitc, ASoile) from LPJmL. Analogously to LPJmL, a further division of Soile into a fast respiring fraction (10 % Soile_{fast}) and a slow respiring fraction (90 % Soile_{slow}) was calculated. Additionally, the annually produced litter prior to respiration is used in RivCM. Since LPJmL does not account for inun-

dation, which changes respiration, the respiration of litter in (partly) water-saturated soils is calculated within RivCM.

In general, in tropical forests litter falls continuously throughout the year (Müller-Hohenstein, 1981). In forests, where the flooding triggers litter fall, a peak in litter fall occurs during the rising- and high-water stages (Irmiler, 1982). Because this is not accounted for in LPJmL (Sitch et al., 2003), the annual unrespired litter carbon pool provided by LPJmL, $\text{ALitc}_{\text{unresp}}$, was heterogeneously partitioned over 12 months to initialize the monthly litter amount ($\text{Litc}_{\text{unresp}}$) in RivCM (Fig. 2, INPUT box). With Eqs. (4) and (5) the maximum amount of carbon was distributed to the month with high water and the minimum (at least 10 % of annual litter) was distributed to the month with low water. This depended on the distance between the current month and the month with high-water peak and the month with low-water peak ($\text{dist}_{\text{highlow}}$). With this approach we achieved a skewed distribution of litter carbon. The factor for the monthly fraction (fraction_{m_t}) was calculated with

$$\text{fraction}_{m_t} = \cos \left(\frac{m_t}{\text{dist}_{\text{highlow}}} \times \pi \right) + (1.0 + \text{litfrac}_{\text{min}}) \quad (4)$$

if the current month number (m_t ; from 0 to 11) is smaller than the distance between high- and low-water peak ($\text{dist}_{\text{highlow}}$)

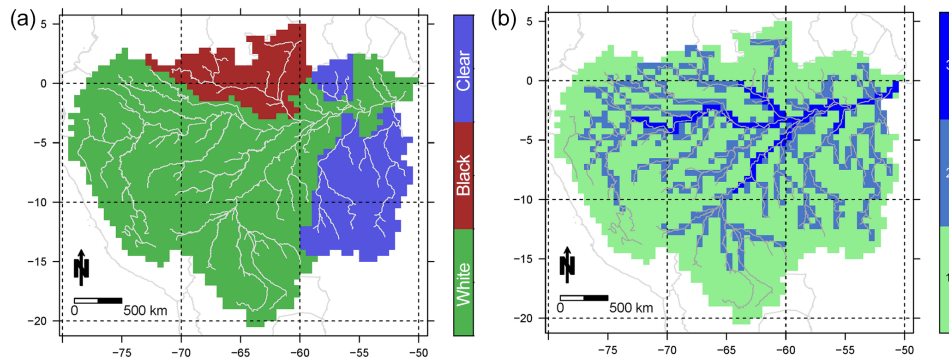


Figure 3. River type (a) and river order (b). Cells of river order 1 (headwater) have a mean annual discharge of less than $8 \times 10^3 \text{ m}^3 \text{ yr}^{-1}$; cells of river order 2 have a discharge between 8×10^3 and $2 \times 10^5 \text{ m}^3 \text{ yr}^{-1}$; cells of river order 3 have a discharge higher than $2 \times 10^5 \text{ m}^3 \text{ yr}^{-1}$.

to distribute the maximum amount of carbon to the month with high water or with

$$\text{fraction}_{m_t} = -\cos\left(\frac{m_t - \text{dist}_{\text{highlow}}}{12 - \text{dist}_{\text{highlow}}} \times \pi\right) + (1.0 + \text{litfrac}_{\text{min}}) \quad (5)$$

if the current month number (m_t ; from 0 to 11) is larger than the distance between high- and low-water peak ($\text{dist}_{\text{highlow}}$) to distribute the minimum amount of carbon ($>= 10\%$ of annual litter) to the month with low water. Equation (4) calculates the convex part of the function, while Eq. (5) calculates the concave part of the function. The first part of both equations represents the cosine portion, and the second part sets the minimum of litter for the month with the low-water peak $\text{litfrac}_{\text{min}}$.

By calculating the fraction of current monthly litter production versus total litter production in the course of each year (Eq. 6), the total monthly unrespired litter carbon ($\text{Litc}_{\text{unresp}t}$) can be determined with Eq. (7).

$$\text{mfraction}_t = \frac{\text{fraction}_{m_t}}{\sum_{t=0}^{11} \text{fraction}_{m_t}} \quad (6)$$

$$\text{Litc}_{\text{unresp}t} = \text{mfraction}_t \times \text{ALitc}_{\text{unresp}} \quad (7)$$

Respiration of litter and soil carbon

The initialized litter and soil carbon pools (Litc , Soilc) are respired and refilled with the amount of the respiration of unrespired litter carbon ($\text{Litc}_{\text{unresp}}$). The calculation of respiration of organic matter depends on soil water content and temperature. The soil water content (Mswc) in uninundated grid cells was provided by LPJmL, while the soil water content of (partly) inundated cells was calculated depending on the fraction of cell covered with water in RivCM. In inundated parts of the grid cell the soil water content was set to 100%. The respiration of the unrespired litter carbon and the soil carbon was calculated analogously to the LPJmL routine (for details, see also Supplement Eqs. S1 to S12) and is updated in each time step.

Mobilization

The mobilization function calculates the amount of mobilized terrestrially fixed carbon dependent on the amount of available exportable organic carbon on land and on the size of inundated area. This area is determined using current discharge, reference discharge and potentially floodable area. The mobilization is not dependent on the river type, since the physical conditions of moving water to mobilize terrigenous material are the same on black- and white-water rivers.

Size of monthly inundated area

The inundated area at time t (InunArea_t (km^2)) was defined as the area covered by water, including river and floodplain. It is determined by the current monthly discharge (Mdis_t ($\text{m}^3 \text{ s}^{-1}$)) relative to the mean maximum discharge of the reference period 1971–2000 (RefMeanMaxMdis ($\text{m}^3 \text{ s}^{-1}$)) produced under the climate forcing of CRU TS2.1 (Österle et al., 2003; Mitchell and Jones, 2005). The potentially floodable inundated area (MaxInunArea (km^2)) (Langerwisch et al., 2013) (Eq. 8) was calculated using the fraction of the cell that is potentially floodable (Langerwisch et al., 2013) multiplied by the cell area. The potentially floodable area was calculated by applying a modified Topographic Relative Moisture Index (based on Parker, 1982) to a digital elevation model provided by the WWF database HydroSHEDS (WWF HydroSHEDS, 2007) as described by Langerwisch et al. (2013).

$$\text{InunArea}_t = \frac{\text{Mdis}_t}{\text{RefMeanMaxMdis}} \times \text{MaxInunArea} \quad (8)$$

If the current monthly discharge is very high and thereby larger than the mean maximum discharge of the reference period, the inundated area can exceed the potentially floodable area.

Because the export of terrigenous organic material is highest close to the river, each cell is subdivided into six sections,

to account for spatial differentiation depending on the vicinity to the river. The size of the sections one to five is calculated with an exponential function (Eq. 9). The remaining cell area is allocated to section six. The river area is assigned to the cell sections starting from the smallest section (Fig. S1 in the Supplement). The river can expand into the next larger section during rising water. The largest section has the largest distance to the river and is therefore only occasionally inundated.

$$\text{size}_{\text{section}} = \frac{1}{e^{(\text{number}_{\text{section}}+1)}} \quad (9)$$

Size of floodplain area

The floodplain area (FloodplainArea (km²)) at time t equals the inundated area that is not permanently covered with water. It was calculated by subtracting the river area (25 % of inundated area, Richey et al., 2002) from the inundated area using Eq. (10) (see also Langerwisch et al., 2013).

$$\text{FloodplainArea}_t = \text{InunArea}_t - (0.25 \times \text{MaxInunArea}) \quad (10)$$

Amount of exported litter and soil carbon

This function calculates the amount of carbon exported from the terrestrial litter and soil pools to the river. River and forests at the headwater, which is defined by an annual discharge of less than $8 \times 10^3 \text{ m}^3 \text{ yr}^{-1}$ (river order 1 in Fig. 3b), are assumed to be much more closely interconnected than at middle and lower reaches (order 2 and 3). Since small streams at the headwater directly flow beneath the trees, their export of litter and soil carbon was calculated from the entire inundated area. In all cells of higher river orders the export of terrestrial organic material occurs in the model only from the floodplain area and not from the permanently flooded river.

The *igapó* forests which are inundated by black-water rivers produce approximately 35 % less litter and soil carbon (Worbes, 1997) compared to white-water-inundated *várzea* forests. LPJmL simulates tropical rainforest, which is analogous to *várzea*. Since LPJmL does not account for the different forest types, a correction of the organic material is performed for the *igapó* forests. Hence, the amount of exportable organic material from the black-water cells at time t is reduced by a factor of 0.35 (1-carboncorr; details in Table 3, Eqs. 11 and 12).

$$\text{Litc}_{t_{\text{corr}}} = \text{Litc}_t \times \text{carboncorr} \quad (11)$$

$$\text{Soilc}_{t_{\text{corr}}} = \text{Soilc}_t \times \text{carboncorr} \quad (12)$$

For simplicity the following equations only refer to Litc instead of to the corrected value Litc_{corr} in the case of *igapó*.

The mobilization of litter and soil carbon at time t (mLitc_{*t*}, mSoilc_{*t*}, (10⁶ g C cell⁻¹)) is calculated using the specific mobilization rates for litter and soil carbon (Table 3, Eqs. 13 and

14).

$$\text{mLitc}_t = \text{Litc}_t \times \text{FloodplainArea}_t \times \text{mobil}_{\text{litc}} \quad (13)$$

$$\text{mSoilc}_t = \text{Soilc}_t \times \text{FloodplainArea}_t \times \text{mobil}_{\text{soilc}} \quad (14)$$

According to Irmeler (1982), litter carbon is mobilized at a rate of 0.4 month⁻¹. After a sensitivity analysis this rate (mobil_{litc}) was calibrated to 0.7 month⁻¹ (see the Supplement). Soil carbon mobilization takes place at a much smaller rate. Since no detailed value is available, the rate of soil mobilization (mobil_{soilc}) was calibrated after a sensitivity analysis to 0.05 month⁻¹. Mobilized carbon (10⁶ g C cell⁻¹), originating from litter and soil, consists of a particulate (mPOC_{*t*}) and a dissolved (mDOC_{*t*}) organic carbon pool with the fractions of mobil_{*p*} and (1.0–mobil_{*p*}), respectively (Table 3, Eqs. 15 and 16).

$$\text{mPOC}_t = (\text{mLitc}_t + \text{mSoilc}_t) \times \text{mobil}_p \quad (15)$$

$$\text{mDOC}_t = (\text{mLitc}_t + \text{mSoilc}_t) \times (1.0 - \text{mobil}_p). \quad (16)$$

The fraction of mobilized particulate carbon (mobil_{*p*}) was set to 0.5 according to McClain and Elsenbeer (2001) and Johnson et al. (2006) and was evaluated in a sensitivity analysis (see the Supplement).

Decomposition

Depending on the rate of decomposition (decomp (month⁻¹), Table 3), the model calculates the conversion from particulate (mPOC_{*t*}) into dissolved organic carbon (dDOC_{*t+1*}), which has been estimated to be about 0.3 month⁻¹ by Furch and Junk (1997). In the calculations this rate was modified according to the river type. Along black-water rivers the leaves are more sclerophyllous and thus much more slowly degradable (Furch and Junk, 1997). Therefore, the decomposition rate in black-water cells is reduced by a factor of 0.9 (1.0–decompcorr) based on Furch and Junk (1997) (Table 3). The decomposed particulate organic carbon at time t , dPOC_{*t*} (Eq. 17), was removed from the particulate organic carbon pool and added to the dissolved organic carbon pool (Eqs. 18 and 19). The dissolved organic carbon is not fragmented any further.

$$\text{dPOC}_t = \text{mPOC}_t \times \text{decomp} \times \text{decompcorr} \quad (17)$$

$$\text{dPOC}_{t+1} = \text{mPOC}_t - \text{dPOC}_t \quad (18)$$

$$\text{dDOC}_{t+1} = \text{mDOC}_t + \text{dPOC}_t \quad (19)$$

Respiration

The respiration function calculates the decrease in particulate and dissolved organic carbon (dPOC_{*t+1*}, dDOC_{*t+1*}, (10⁶ g C cell⁻¹)) by the respiration loss (rPOC_{loss} and rDOC_{loss}) and the associated increase in dissolved inorganic carbon (rIC_{*t+1*}) at time t (Eqs. 20 to 24). For this, a sufficient abundance of respiring organisms is assumed. In con-

Table 3. List of parameters.

Parameter name	Value	Unit	Source	Original value
Loss via terrestrial respiration				
respi _{litic}	30	%	LPJmL	
respi _{soilfast}	3	%	LPJmL	
respi _{soilslow}	0.1	%	LPJmL	
respi _{partsoilfast}	98	%	LPJmL	
respi _{partsoilslow}	2	%	LPJmL	
Mobilization				
carboncorr	0.65	month ⁻¹	Worbes (1997)	0.65 ± 0.15
mobil _{litic}	0.7	month ⁻¹	Irmler (1982)	0.4 ± 0.1
mobil _{soilc}	0.05	month ⁻¹	Irmler (1982)	
mobil _p	0.5	–	Johnson et al. (2006); McClain and Elsenbeer (2001)	0.5 ± 0.25
Decomposition				
decomp	0.3	month ⁻¹	Furch and Junk (1997)	0.3 ± 0.1
decompcorr	0.1	month ⁻¹	Furch and Junk (1997)	0.1 ± 0.01
Respiration				
respi	0.04	day ⁻¹	Cole et al. (2000)	0.045 ± 0.01
Outgassing				
co2satur	7.25 to 17.0	–	Richey et al. (2002)	7.25 to 17.0

trast to different decomposition rates in black- and white-water rivers, which is due to the fact that leaves at black-water rivers tend to be more sclerophyllous and therefore less easily degradable, for the respiration of already degraded organic material we assume only minor differences. As soon as the leaves and twigs are degraded to small particles we assume that they react similarly. Therefore, respiration only depends on the rate of respiration loss (respi (month⁻¹), see Table 3) and the temperature response (Tresponse, Eq. 2).

$$rPOC_{loss} = dPOC_{t+1} \times (1 - e^{-(respi \times Tresponse_t)}) \quad (20)$$

$$rDOC_{loss} = dDOC_{t+1} \times (1 - e^{-(respi \times Tresponse_t)}) \quad (21)$$

$$rPOC_{t+1} = dPOC_{t+1} - rPOC_{loss} \quad (22)$$

$$rDOC_{t+1} = dDOC_{t+1} - rDOC_{loss} \quad (23)$$

$$rIC_{t+1} = IC_t + rPOC_{loss} + rDOC_{loss} \quad (24)$$

Outgassing

The model calculates the monthly saturation concentration of CO₂ saturationC_t in the water, Mwat_t (m³) (Eq. 25),

$$saturationC_t = k_H^\theta \times e^{d \ln k_H \times \left(\frac{1}{T_t + 273.15} - \frac{1}{T^\theta} \right)} \times \frac{atmCO_{2t}}{10^6} \times ctoco2 \times Mwat_t \times 10^3, \quad (25)$$

using Henry’s law (Sander, 1999) and applying the Henry’s law constant (k_H^θ (g CO₂ L⁻¹ atm⁻¹)) under standard conditions ($T^\theta = 298.15$ K), the temperature dependence of the

Henry’s law constant (dlnkH (K)), the ratio of carbon to carbon dioxide (ctoco2) and monthly temperature T_t in °C. Depending on the river type, which determines the pH of the water, we calculated the amount of CO₂, HCO₃³⁻ and CO₃²⁻. For calculating the actual outgassing we only take the carbon into account instead of the chemical form in which it exists. Afterwards, monthly saturation is multiplied with a monthly saturation factor (co2satur, Eq. (26), Table 3), which accounts for the supersaturation of the water with CO₂. These values depend on the hydrograph and were extracted from Richey et al. (2002). The difference between inorganic carbon amount and saturation concentration was added to the atmosphere carbon pool (Icoutgas_{t+1}, Eq. 27), while carbon in the river equals the saturation concentration (oIC_{t+1}, Eq. 28).

$$saturationC_{corr_t} = saturationC_t \times co2satur \quad (26)$$

$$Icoutgas_{t+1} = Icoutgas_t + (rIC_{t+1} - saturationC_{corr_t}) \quad (27)$$

$$oIC_{t+1} = saturationC_{corr_t} \quad (28)$$

2.2 Climate data sets

For model evaluation, climate forcing data from a homogenized and extended CRU TS2.1 global climate dataset (Österle et al., 2003; Mitchell and Jones, 2005) were used. Annual atmospheric CO₂ concentrations were prescribed as given by Keeling and Whorf (2003).

For the assessment of climate change impacts, three Special Report on Emissions Scenarios (SRES) scenarios (A1B, A2, B1) (Nakićenović et al., 2000) were applied. Five General Circulation Models (GCMs) (Jupp et al., 2010;

Table 4. List of data used for calibration and validation.

	Observation	Simulated	Diff	Source
Annually outgassed CO ₂				
Basin-wide (10 ¹⁴ g C yr ⁻¹)	4.7	1.28	-73 %	Richey et al. (2002)
In central part* (10 ¹⁴ g C yr ⁻¹)	2.1 ± 0.6	0.51	-76 %	Richey et al. (2002)
Per km ² (10 ⁸ g C km ⁻² yr ⁻¹)	1.2 ± 0.3	0.21	-82 %	Richey et al. (2002)
	6.4 ± 6.0	0.21	-96.7 %	Abril et al. (2014)
	8.0 ± 1.8	0.21	-97.4 %	Belger et al. (2011)
	60 ± 6.8	0.21	-99.7 %	Neu et al. (2011)
Annually exported carbon to Atlantic Ocean (estimated at Óbidos) (10 ¹⁴ g C yr ⁻¹)				
TOC*	0.36 ± 0.1	0.64	+80 %	Richey et al. (1990); Moreira-Turcq et al. (2003)
POC	0.12 ± 0.05	0.19	+63 %	Junk (1985); Moreira-Turcq et al. (2003)
DOC	0.27	0.45	+67 %	Moreira-Turcq et al. (2003)
Annually exported carbon from sub-catchments (10 ¹² g C yr ⁻¹)				
POC				
Vargem Grande	6.4	8.3	+30 %	Richey and Victoria (1993)
Rio Madeira	3.2	7.4	+31 %	Richey and Victoria (1993)
Óbidos	12.1	19.4	+20 %	Richey and Victoria (1993)
DOC				
Vargem Grande	4.7	21.0	+347 %	Richey and Victoria (1993)
Rio Negro	6.6	09.2	+39 %	Richey and Victoria (1993)
Rio Madeira	2.6	17.5	+573 %	Richey and Victoria (1993)
Óbidos	18.4	45.1	+91 %	Richey and Victoria (1993)
Carbon concentration (10 ⁻³ g C l ⁻¹)				
TOC*	9.85 ± 4.5	7.46	-24 %	Ertel et al. (1986); Moreira-Turcq et al. (2003)
POC (average)	1.50 ± 0.5	2.16	+44 %	Moreira-Turcq et al. (2003)
Rio Negro	0.69 ± 0.16	1.85 ± 1.33	+170 %	Moreira-Turcq et al. (2003)
Rio Negro	0.37 ± 0.17	0.16	-58 %	Richey et al. (1990)
Rio Branco	0.71 ± 0.28	2.03 ± 0.67	+190 %	Moreira-Turcq et al. (2003)
Rio Solimões	1.26 ± 0.47	0.66 ± 0.61	-48 %	Moreira-Turcq et al. (2003)
Rio Madeira	1.73 ± 1.8	1.42 ± 1.39	-18 %	Moreira-Turcq et al. (2003)
Rio Madeira	2.87 ± 1.24	1.70	-41 %	Richey et al. (1990)
Rio Japura	1.88 ± 0.39	1.02	-46 %	Richey et al. (1990)
Itapeva	3.21 ± 0.52	1.80	-44 %	Richey et al. (1990)
Óbidos	2.41 ± 0.39	0.13	-87 %	Richey et al. (1990)
DOC (average)	7.35 ± 4.0	5.30	-28 %	Ertel et al. (1986); Hedges et al. (1994); Moreira-Turcq et al. (2003)
Rio Negro	11.61 ± 5.49	2.07 ± 1.42	-82 %	Moreira-Turcq et al. (2003)
Rio Negro	8.43 ± 1.20	0.38	-95 %	Richey et al. (1990)
Rio Branco	2.4	2.25 ± 0.75	-6 %	Moreira-Turcq et al. (2003)
Rio Solimões	4.26 ± 1.67	1.52 ± 1.32	-64 %	Moreira-Turcq et al. (2003)
Rio Madeira	4.31 ± 2.23	7.16 ± 5.49	+66 %	Moreira-Turcq et al. (2003)
Rio Madeira	3.49 ± 1.18	0.40	+88 %	Richey et al. (1990)
Rio Japura	3.46 ± 0.66	2.44	-29 %	Richey et al. (1990)
Itapeva	3.76 ± 0.83	3.82	+2 %	Richey et al. (1990)
Óbidos	4.03 ± 0.70	0.74	-82 %	Richey et al. (1990)
IC (average)	0.95–4.08	1.64	-70 – +60 %	Neu et al. (2011); Richey et al. (2002)
Vargem Grande	1.12	1.84	+64 %	Devol et al. (1987)
Rio Ica	2.07	1.78	-14 %	Devol et al. (1987)
Rio Juruá	2.71	2.67	-02 %	Devol et al. (1987)
Jutica	1.77	1.72	-03 %	Devol et al. (1987)
Manacapuru	1.79	1.64	-08 %	Devol et al. (1987)
Rio Negro	1.44	1.72	+20 %	Devol et al. (1987)
Rio Madeira	2.34	1.75	-25 %	Devol et al. (1987)
Óbidos	1.98	1.69	-15 %	Devol et al. (1987)
Willmott's index of agreement				
Calibration data*	Before calibration	0.870	After calibration	0.893
Other data		0.413		0.635
All data		0.427		0.615

Comparison of observed values with results of the simulations using initial parameter setting (before calibration) and calibrated parameter setting. Difference (diff) is relative difference to observation (%). A Willmott's index of agreement of 1.0 indicates full agreement.

* indicates data used for calibration.

see also Randall et al., 2007), namely, MIUB_ECHO_G, MPI_ECHAM5, MRI_CGCM2_3_2a, NCAR_CCSM3_0 and UKMO_HADCM3, were chosen to cover a wide range of uncertainty within climatic projections with respect to precipitation patterns and temperature. The GCMs used the SRES scenarios to calculate future climate. For example, the model MIUB_ECHO_G shows a shortening of the dry season (defined by less than 100 mm precipitation per month), whereas UKMO_HADCM3 shows an extension of the dry season towards the end of the century. Temperature in the Amazon basin is projected to increase under the A1B emission scenario by about 3.5 K, by up to 4.5 K for A2 and by up to 2 to 2.5 K for B1 until the end of the century (Meehl et al., 2007). Projected rainfall differs considerably in spatial distribution within the Amazon basin among climate models. Under A1B, for instance, a decrease in precipitation is projected for southern Amazonia (especially during the Southern Hemisphere winter), whereas an increase in precipitation is projected in the northern part (for details, see Meehl et al., 2007). The projected climate data were bias-corrected with the CRU TS2.1 global climate dataset (Österle et al., 2003; Mitchell and Jones, 2005). Annual future atmospheric CO₂ concentrations are based on the respective SRES scenario.

All monthly climate data (observed and projected) were disaggregated to “quasi-daily” values as described by Gerten et al. (2004).

2.3 RivCM calibration and evaluation

To identify the most important explaining variables (parameters) and the most sensitive response variables (carbon pools), a redundancy analysis (RDA) was performed. Based on the analysis, we calibrated mobil_{litc} and mobil_{soilc} (see the Supplement).

To evaluate the performance of RivCM, a comparison of observed with simulated data was conducted. TOC, POC and DOC concentration were chosen, as was exported carbon to the ocean (TOC, POC and DOC per year) and exported carbon to the atmosphere (outgassed CO₂ per year in different spatial domains) (see Table 4). The estimates of carbon exported to the Atlantic Ocean are from the gauging station at Óbidos. The data from this station represent an integration of information over the entire Amazon basin. Therefore, they do not reflect large temporal or spatial deviation over the basin and enable us to compare aggregated measured data with aggregated simulated data. If possible, data from the same time period were compared. If the observation period was after the last simulation year 2003, the data were compared to simulated values from the reference period (1971–2000). Additional results of the evaluation can be found in the Supplement.

2.4 Modelling protocol and simulation experiments

We performed LPJmL simulations with potential natural vegetation only, i.e. without land use, on a 0.5° × 0.5° spatial resolution. To obtain equilibria for vegetation distribution, carbon and water pools in LPJmL, all transient LPJmL runs were preceded by a 1000-year spinup during which the pre-industrial CO₂ level of 280 ppm and the climate of the years 1901–1930 were repeated. All transient runs of the coupled model LPJmL–RivCM were preceded by a 90-year spinup during which the climate and CO₂ levels of 1901–1930 were repeated to obtain equilibria for riverine carbon pools. Transient climate simulations are then performed for current climate (1901–2003) and future climate (2004–2099). The data sets used are described in Sect. 2.2.

To identify how relevant the amount of riverine outgassed carbon for the basin-wide carbon budget in a changing climate is, we compared the output of coupled terrestrial–riverine modelling runs with purely terrestrial or purely riverine modelling settings. The three different factorial settings are the following:

Setting 1 (Standard) refers to the standard RivCM simulation, including the actual river and the additionally inundated area. In these simulations the export of organic material from the land to the river was calculated, as well as the discharge of carbon to the ocean, aquatic outgassing and the release of CO₂ via terrestrial heterotrophic respiration.

Setting 2 (NoInun) includes the actual river but excludes additional inundation. For this purpose, the cell fraction which is not permanently covered by water remains dry to emulate no coupling of land and river. In this simulation experiment no export of organic material from the land to the river was calculated (i.e. there is no input of terrigenous organic material into the river). Hence, no discharge of carbon to the ocean and no outgassing was calculated, but release of CO₂ from the terrestrial heterotrophic respiration was.

Setting 3 (NoRiv) includes calculations in which the original LPJmL results for CO₂ release from vegetation only were used, i.e. the influence of the river and inundation were not accounted for. In these simulations no outgassing from the water and no discharge of carbon to the ocean was calculated. In contrast, outgassing from the heterotrophic respiration of the forest, also in the areas in which RivCM simulates river area, was calculated.

In a full factorial design, all inundation scenarios (Standard, NoInun and NoRiv) were run for all climate scenarios for future and current climate.

2.5 Analyses of future changes in the coupled terrigenous–riverine system

The effect of climate change is estimated by calculating the differences between carbon values in a future period (2070–2099) and a reference period (1971–2000). Four different carbon pools were analysed, namely outgassed carbon (at-

Table 5. Location and characteristics of the three subregions.

	North-west corner	South-east corner	Area (10 ³ km ²)	Changes in inundation length*	Changes in inundated area*
R1	0.5° S, 78.5° W	7.0° S, 72.0° W	523.03	1 month longer	Larger
R2	1.0° S, 70.0° W	5.0° S, 52.0° W	891.32	± 1/2 month shift	Heterogeneous
R3	4.5° S, 58.0° W	11.0° S, 52.0° W	523.03	1/2 shorter	Smaller

Regions are also depicted in Fig. 6a. * Changes in inundation compared to the average of 1961–1990, as estimated and discussed in Langerwisch et al. (2013).

mospheric), riverine particulate organic carbon (POC) and dissolved organic carbon (DOC), as well as the riverine inorganic carbon pool (IC). The relative changes in POC and DOC are spatially and temporally similar (Fig. S4 in the Supplement). Therefore, only POC is shown and discussed in detail.

The spatial distribution of climate change effects (E_{CC}) on the different carbon pools and fluxes (indicated by n) were estimated by calculating the quotient (Eq. (29) of future values (mean of 2070–2099) and reference values (mean of 1971–2000) for each cell. To equalize a 10-fold increase (10^{+1}) and a reduction to 1/10 (10^{-1}), the quotient was log-transformed (\log_{10}).

$$E_{CC_n} = \log_{10} \frac{\sum_{n=2070}^{2099} C_n}{\sum_{n=1971}^{2000} C_n} \quad (29)$$

To show the model uncertainty that arises from differences in climate model projections, an indicator of the agreement between simulation results was calculated; it indicates a common significant increase or decrease in three, four or all five climate models. In addition, the significance (p value < 0.05) of the difference between reference and future was assessed by a Wilcoxon rank-sum test (Bauer, 1972). This test can be used for datasets that are not normally distributed and is therefore applicable to these data with high intra-annual fluctuations.

Additionally to the analysis of spatial patterns, an analysis of changes in mean carbon pools over time was conducted. As above, changes were expressed as the logarithm of the quotient between annual future values and mean reference values. In addition to these relative changes, the absolute values in both periods were compared. The analysis was conducted both for the whole Amazon basin and for three selected subregions. These three regions, indicated in Fig. 6a, were identified according to future changes in inundation patterns, discussed in Langerwisch et al. (2013). These areas include a region in the western basin with a projected increase in inundation length and inundated area (R1), a region covering the Amazon main stem (R2) with intermediate changes in inundation, and a region with a projected decrease in the duration of inundation and inundated area (R3). For details of the exact position and the characteristics of these regions see Table 5.

All statistical analyses were conducted using several packages in R. For the sensitivity analysis the package “vegan” was used (Oksanen et al., 2011), and for the analysis of the projections the packages “stats” (R Development Core Team and contributors worldwide, 2011) and “maptools” (Lewin-Koh and Bivand, 2011) were used.

3 Results

3.1 Validation of the simulation results

To assess the potential changes in the riverine carbon pools and fluxes, it is essential that we trust the model’s ability to reproduce observed patterns and fluxes. For this, the first step is to validate river discharge before assessing carbon pools and fluxes. This has been done in Langerwisch et al. (2013) for 44 gauging stations in the Amazon basin and shows that the observed discharge patterns can be reproduced. Here, we validated the carbon concentration and export fluxes with published data (Table 4). If possible, we compared the simulated with observed values from the same period of time. We only included spatial data for which we could find the exact location (latitude/longitude).

The validation of exported data shows that the outgassed carbon (export to the atmosphere) is underestimated by the model on a small scale by more than 90 % and on the basin-wide scale by 70 %. In contrast the organic carbon exported to the ocean is overestimated by the model by 70 %. However, on a sub-catchment level the overestimation of exported organic carbon is much smaller. Comparing observed and simulated concentrations of POC, DOC and IC shows that simulation results are within the observed range. For POC the simulated concentration is about 50 % larger than the observed concentration but with a range between –90 % and +200 %. For the simulated DOC concentration the range is between –90 and +90 %, while for IC the range is between –70 and +60 %.

3.2 Changes in riverine carbon under future climate projections

The amount of outgassed carbon (Fig. 4a) is simulated to remain constant compared to 1971–2000 until about 2020. This is followed by a clear increase. This increase is strongest in region R1 (mean +70 %), while it is moderate in R2 and R3 (+30 and +20 %, respectively). Generally, the simulated in-

Table 6. Mean annual export of carbon during reference and future period.

TOC discharge to ocean			Outgassed carbon to atmosphere						
			Standard ^a		NoInun ^b		NoRiv ^c		
Sum (10 ¹² g yr ⁻¹)	Prop. of NPP (%)	sum _{std} (10 ¹² g yr ⁻¹)	Terr. (10 ¹² g yr ⁻¹) (% of sum _{std})	Riv. (10 ¹² g yr ⁻¹) (% of sum _{std})	Prop. of NPP (%)	Sum 100 % terr. (10 ¹² g yr ⁻¹)	Rel. to sum _{std} (%)	Sum 100 % terr. (10 ¹² g yr ⁻¹)	Rel. to sum _{std} (%)
Basin-wide									
Reference period									
54.1	1.0	5271.6	5081.8 (96.4)	189.8 (3.6)	3.5	5097.6	-3.3	5266.8	-0.10
Future period									
A1B	49.3	6469.2	6204.0 (95.9)	265.2 (4.1)	4.0	6258	-3.3	6463.2	-0.10
Prop. to ref A2	(-8.9)	(+22.7)	6463.2 (95.7)	290.4 (4.3)	4.2	(+22.8) 6534.0	-3.2	(+22.7) 6748.8	-0.07
Prop. to ref B1	(+9.1)	(+28.1)	6163.6 (96.1)	248.8 (3.9)	3.9	(+28.2) 6172.8	-3.3	(+28.1) 6375.6	-0.07
Prop. to ref	(+4.6)	(+21.0)				(+21.1)		(+21.1)	
Main stem (R2)									
Reference period									
		784.8	745.6 (95.0)	39.2 (5.0)	4.9	753.6	-4.0	780	-0.61
Future period									
A1B		925.2	873.4 (94.4)	51.8 (5.6)	5.7	888.0	-3.9	920.4	-0.54
Prop. to ref A2		(+17.8) 960.0	903.4 (94.1)	56.6 (5.9)	6.1	(+17.9) 921.6	-3.9	(+17.9) 954	-0.54
Prop. to ref B1		(+22.3) 930.0	880.7 (94.7)	49.3 (5.3)	5.6	(+22.3) 892.8	-3.9	(+22.2) 925.2	-0.53
Prop. to ref		(+18.4)				(+18.5)		(+18.5)	

Mean annual export of carbon in reference period (1971–2000) and future period (2070–2099), averaged over five climate models. List of discharged total organic carbon into the Atlantic Ocean and basin-wide monthly outgassed carbon produced via heterotrophic respiration. NPP is net primary production. Proportional differences (%) between reference and future period are in round brackets. Differences in total outgassed carbon between future and reference values are in all cases highly significant (Wilcoxon rank-sum test; $p < 0.001$). Negative (positive) values indicate a decrease (increase) compared to the Standard simulations.

^a Standard RivCM simulations.

^b RivCM simulation without additional inundation (NoInun); therefore no export of terrigenous organic carbon.

^c LPmL calculating forest instead of river (NoRiv). For details of river area calculation, see Langerwisch et al. (2013).

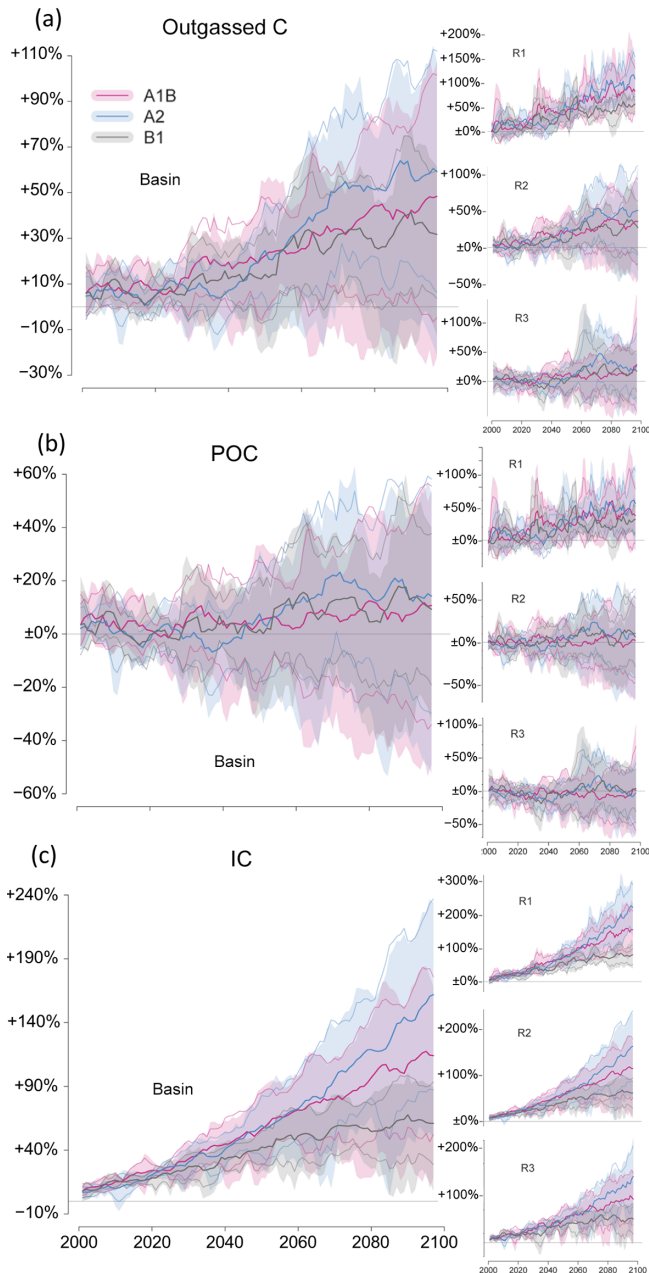


Figure 4. Temporal change in riverine carbon pools caused by climate change. Panel (a) shows results for outgassed carbon, (b) for particulate organic carbon (POC) and (c) for inorganic carbon. Results are shown as the quotient of annual carbon amount and mean annual carbon amount in reference period for the whole basin and the three subregions (R1–R3). Different colours represent different SRES emission scenarios. The shaded area for each scenario is spanned by the minimal and maximal values of all five climate models and scenarios. Bold lines represent the 5-year mean for the climate models and scenarios, and thin lines represent mean ± 1.0 standard deviation. Positive values indicate an increase in outgassed CO_2 in the future compared to reference period, and negative values indicate a decrease. The horizontal line at $y = 1$ indicates no change compared to the reference period 1971–2000.

crease is largest for the SRES A2 scenario, followed by the A1B and the B1 scenario (see also Fig. 5). The spread of simulated outgassed carbon is comparably large between the five climate models. Outgassed carbon shows a basin-wide increase (Fig. 6g–i). In most parts of the basin the outgassed carbon increases only slightly but significantly ($p < 0.05$; up to 2-fold). In parts of the Andes the increase is up to 5-fold, shown by at least four of the five climate models (as indicated by crosses in Fig. 6). In a few areas in the Southern Andes the outgassed carbon decreases (0.3-fold).

The changes in POC (Fig. 4b) show a slight basin-wide increase of about +10 % (SRES mean) until the end of the century. In region R1 this increase is larger, with +50 % (SRES A2) and +35 % (SRES B1). In the regions R2 and R3 the POC amounts remain nearly constant (+5 and ± 0 %, respectively). A wide range of possible paths of simulated POC amounts is spanned by the five climate models, whereas the three emissions scenarios only result in minor differences in simulation results (see also Fig. 5). The spatial changes for POC show an increase up to 2-fold in the western and south-western part of Amazonia for all three SRES emissions scenarios (Fig. 6a–c) with high agreement between the five climate models compared to the reference period. In contrast, climate model agreement in the northern and north-western basin is lower and shows a decreasing trend in the POC pool with a factor of 0.5. For the central part of the basin, no clear trend is visible. POC seems to be less sensitive to different changes in atmospheric CO_2 concentrations compared to IC as only small regional differences were simulated with POC increasing in the western part of the basin under the A2 scenarios and decreasing in the northern part of the basin under the A1B scenario.

In contrast to outgassed carbon and DOC, riverine inorganic carbon (IC) increases basin-wide (Figs. 4c and 5) during the entire 21st century. Here, clear differences in the SRES emission scenarios are found. In the SRES A2 scenario the increase is largest, with a basin-wide increase of +150 % (+220 % in R1, +150 % in R2 and +140 % in R3). In the B1 scenario the average increase is smallest, with basin-wide +50 % (+80 % in R1, +60 % in R2 and +50 % in R3). The spatial distribution of changes in riverine inorganic carbon (IC, Fig. 6d–f) shows an overall increase compared to the reference period. For at least four climate models this increase in IC is significant ($p < 0.05$), especially in the western part of the basin. Here, the largest changes are found for the SRES emission scenario A2 (up to 5-fold increase).

3.3 Changes in the export of riverine carbon to ocean and atmosphere under future climate

Riverine outgassed carbon makes up on average 10 % of total outgassed carbon along the river network during the reference period (Fig. 7a). Total outgassed carbon includes carbon evaded from the river and the forest. The carbon evaded from the forest reflects the amount of terrestrial respired car-

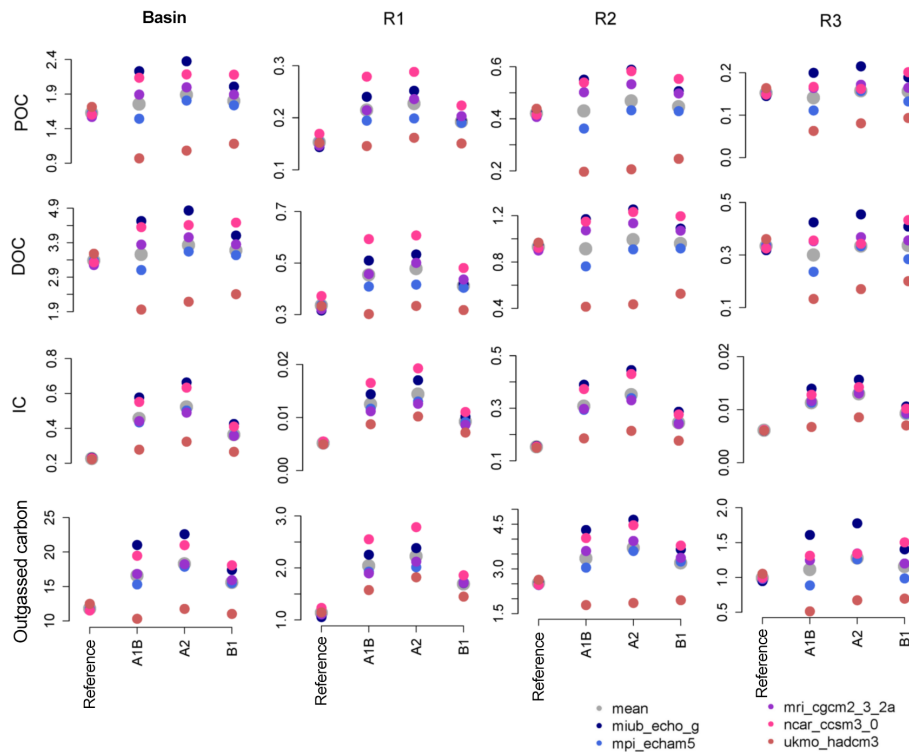


Figure 5. Mean annual sums of carbon pools (10^{12} g) for the whole basin and three subregions for the reference period (1971–2000) and the future period (2070–2099, SRES A1B, A2 and B1). Each for five climate models and scenarios.

bon (autotrophic and heterotrophic respiration). The average changes in this proportion caused by climate change and the agreement of climate models (indicated by crosses) in the direction of change are depicted in the three maps in Fig. 7b–d. The largest differences are found under the SRES A2 scenario with the largest area in agreement between the climate models (Fig. 7c). Here an increase of up to 7% in the proportion is found in the western and south-western part of the Amazon basin. This increase is less pronounced in the other two emission scenarios (Fig. 7b and d). For all SRES scenarios a slight decrease in the proportion of up to 2% (-0.02) can be seen in parts of the north-western basin and scattered in the very south (Fig. 7b–d); this occurs because rivers will contribute increasingly to respiration losses of carbon.

To estimate the relevance of riverine carbon to imported atmospheric carbon (via terrestrial photosynthesis) or exported carbon (via outgassing or discharge to the ocean), results of the factorial experiments were compared (Wilcoxon rank-sum test; $p < 0.001$, Table 6; see also Sect. 2.4). The standard RivCM results (Standard) were analysed to estimate the role of riverine carbon to total carbon export. The simulated mean annual total organic carbon (TOC) discharged to the ocean during the reference period (1971–2000) is about $54 \times 10^{12} \text{ g yr}^{-1}$ (Table 6). This represents approximately 1.0% of the basin NPP. The export of TOC to the ocean under climate change depends on the three SRES emission sce-

narios. In the A1B scenario mean annual export decreases significantly by about 8.9% for 2070–2099 (compared to the reference period) for all five climate models, whereas under the A2 scenario the TOC export increases by about +9.1%. The B1 scenario shows an intermediate change, with an increase of about +4.6%. Depending on the emission scenario, the export of TOC to the ocean decreases from about 1% of the NPP to about 0.75–0.9% of the NPP in the future period.

3.4 Summary of overall changes in the carbon fluxes under climate change

The first three research questions we addressed in this study were answered with the above-mentioned results. As a summary, Fig. 8 provides an aggregated picture of projected changes in terrestrial carbon pools and resulting changes in riverine carbon pools. The moderate increase in terrestrial carbon (on average +12.7% in biomass, +13.8% in litter carbon and +4.1% in soil carbon) leads to a moderate increase in riverine organic carbon (POC +10.7% and DOC +8.3%), but due to an increased CO_2 partial pressure the outgassed carbon increases by about 42.6%, whereas the discharged carbon only increases by about 1.1%.

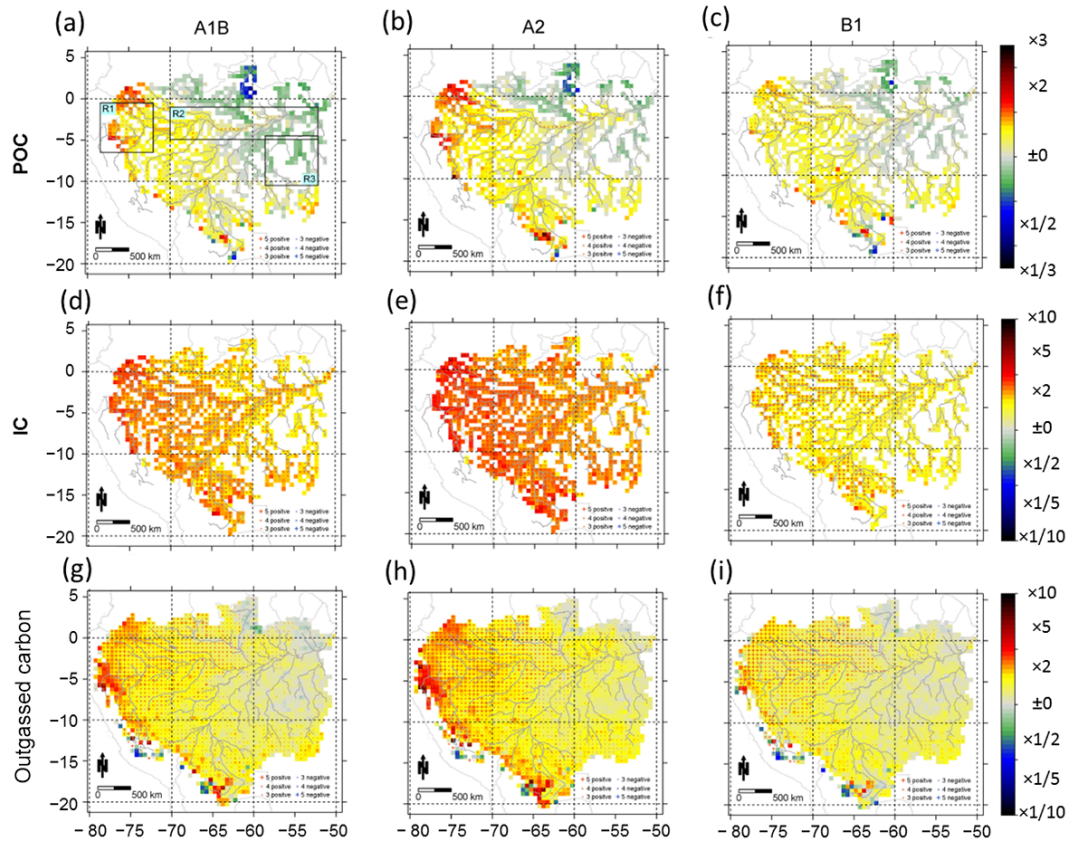


Figure 6. Change in riverine and outgassed carbon caused by climate change. Model mean of the relative increase and decrease in future mean and reference mean of POC (a–c) and IC (d–f) and outgassed carbon (g–i). Left-hand side panels (a, d, g) show the mean of the quotient for SRES A1B emission scenario, middle panels (b, e, h) that for A2 and right-hand side panels (c, f, i) that for B1, averaged over five climate models and scenarios. Positive values (yellow and red) indicate an increase and negative values (green and blue) indicate a decrease. Additionally to the mean, the number of climate models and scenarios leading to significant trends ($p < 0.05$, Wilcoxon rank-sum test) is indicated by crosses. In white cells the differences between future and reference values are not significant.

3.5 Relevance of the riverine outgassed carbon

To assess the relevance of riverine carbon for total carbon export to the atmosphere, either from the forest (heterotrophic respiration) or from the water, the standard RivCM results (Standard) were compared to results of the NoInun experiment and the NoRiv experiment (Table 6). In the reference period the total outgassed carbon is estimated to be about $440 \times 10^{12} \text{ g month}^{-1}$, calculated in the standard RivCM simulations (Standard). Under climate change this amount increases by 23, 28 and 21 % for emission scenarios A1B, A2 and B1, respectively. The proportion of outgassed carbon from the river to total outgassed carbon is about 3.6 % in the reference period. This proportion increases in all emission scenarios to up to 3.9 to 4.3 %. During the reference period the amount of riverine outgassed carbon makes up about 3.5 % of the NPP. In the future this proportion increases significantly to up to 4.25 %.

The simulations without input of terrigenous organic material to the river, caused by suppressed inundation (NoInun),

lead to a reduction in total outgassed carbon. During the reference period it is significantly reduced by about -3.30% . During the future period this reduction remains relatively constant for all SRES scenarios. If the river area is substituted by potential forest cover (NoRiv), the total terrestrial outgassed carbon is about 0.1 % lower than the sum of terrestrial and riverine outgassed carbon in the standard simulations. This proportion decreases slightly to 0.07–0.10 % in the future period.

4 Discussion

The main goal of our study was to develop a coupled terrestrial–riverine model for assessing regional and global carbon budget, considering riverine carbon pools and fluxes and their potential changes under climate change. We used the Amazon basin as a case study because it represents a tightly coupled terrestrial–riverine system. To achieve our goal we combined the newly developed riverine carbon model RivCM with the terrestrial vegetation model LPJmL.

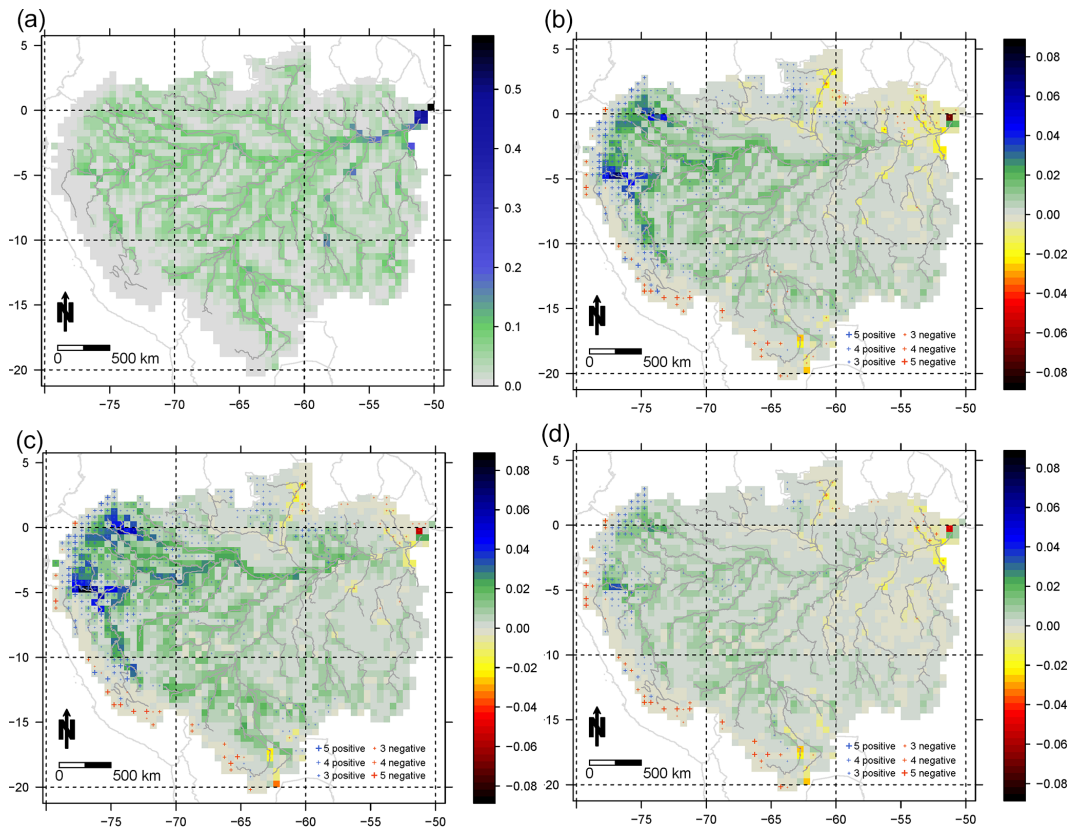


Figure 7. Proportion of outgassed carbon from the river to total outgassed carbon (a) during the reference period (1971–2000) and the difference in this proportion between future (2070–2099) and reference period caused by climate change averaged over five climate models and scenarios in emission scenario A1B (b), A2 (c) and B1 (d); positive values indicate an increase and negative values indicate a decrease in the future period.

In the following we discuss the performance of and uncertainties in the coupled model system, as well as the mechanisms leading to projected changes in riverine carbon. Finally, we elaborate on the importance of incorporating the terrestrial–riverine coupling in models to better understand processes in terrestrial–riverine systems.

4.1 Riverine carbon pools

The model RivCM calculates the dynamics of several organic carbon pools and fluxes in the Amazon basin. A comparison of these carbon pools and fluxes with observation shows in summary that model results are within the range of observed concentrations of both organic and inorganic carbon pools, but the model strongly underestimates the outgassed carbon, while it overestimates the carbon discharged to the ocean.

For the concentration of carbon the range of observations is large, mainly because of the different characteristics of the sub-catchments. The concentration of organic and inorganic carbon is overestimated by the model for some sub-catchments, while it is underestimated for others. The sub-catchments differ in their specific characteristics, such as water, soil and vegetation. Amon and Benner (1996) for in-

stance illustrated the large difference in the mineralization of organic carbon in clear, white and black waters. The model has difficulties with capturing these differences. Thus, including more site-specific information for the water, the vegetation and the characteristics of the river stretch could lead to a better match between observation and simulation. However, the standard deviation of the observation is large and for most of the cases the simulated concentration lies within the observed range. The mismatch between the observation and the simulation may also be caused by an over- or underestimation of carbon exported to the river, which depends on the inundated area. The model takes the non-linear change in inundated area during flooding only into account in a simplified way, which may lead to an underestimation of flooded area. The relatively coarse spatial resolution may also be a reason for the underestimation of the flooded area. The fixed ratio of 25 % of the potentially floodable area, representing the river, may be less applicable to areas in the headwater. We compared the fixed ratio of 25 % against observation in the lowlands (e.g. Lauerwald et al., 2015; Lehner and Döll, 2004; Richey et al., 1990) and think that this ratio is reasonable for the Amazon lowland. However, misestimating the actual

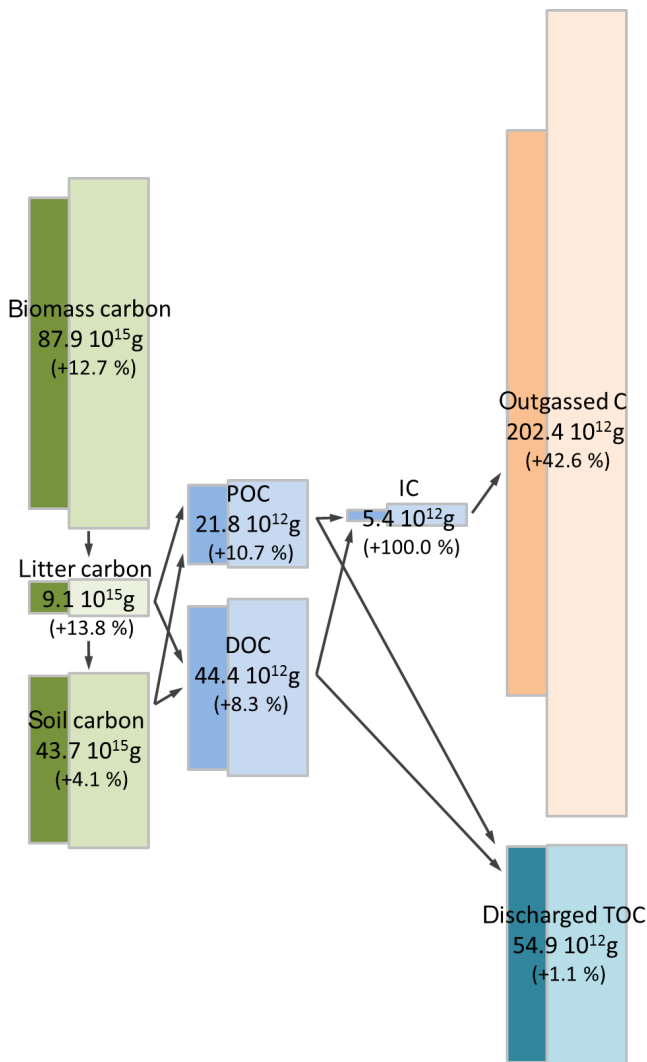


Figure 8. Averaged change in the basin carbon budget due to climate change. Dark boxes indicate the amount of carbon during the reference period and light boxes during the future period (average over all SRES scenarios and GCMs). Amount is given for future period with relative change compared to reference. Arrows indicate the direction of carbon transport.

floodplain river may also lead to poor estimates of exported organic carbon. An additional cause of differences between observed and simulated (inorganic) carbon amount may be that the model does not take weathering, carbon sources other than terrigenous carbon or the longer residence time of water in the flooded forests into account. In summary, the main reasons for the mismatch between observations and simulations are some simplifications (spatially and within the processes) we applied.

For the comparison of exported carbon to either the ocean or the atmosphere the model tends to overestimate the discharge to the ocean, while it underestimates the outgassing. The amount of discharged carbon is tightly coupled to the

concentration and the water discharge. While the discharge of water has been shown to be realistic (Langerwisch et al., 2013), and the simulated concentration is within the observed range, a slight shift in the hydrograph can lead to the mismatch between the observed and simulated amount of carbon exported to the ocean. In addition, the model may overestimate carbon exported to the ocean because it does not include dams. These artificial structures can lead to a prolonged residence time of water and its transported material, and thus to prolonged decomposition and an increased sedimentation (Goulding et al., 2003). In the natural parts, such as floodplains, sedimentation especially impacts the river bed structure (Allison et al., 1995; Junk and Piedade, 1997). However, the sedimentation of organic material is comparably small with only $50 \text{ g C yr}^{-1} \text{ m}^{-2}$ of water area (Melack et al., 2009). Sedimentation and resuspension act on the small to medium scale (Junk and Piedade, 1997; Yarnell et al., 2006). With a spatial resolution of 0.5° , both processes are assumed to be balanced for organic carbon and have therefore not been explicitly calculated in the model but may be of importance on smaller scales. The amount of outgassed carbon from the body of the river to the atmosphere is probably underestimated because the way RivCM calculates the inundated area and thus the area of evasion does not include the cross section of the riverbed. Thus, the non-linear increase in inundated area with an increase in water amount is not included. Including this would potentially lead to a larger inundated area, which would increase the outgassing. The temporal resolution of monthly time steps may also be a reason for the underestimation of the outgassing. In contrast to decomposition and respiration, which are calculated with fixed rates, the outgassing is variable and depends on the prescribed partial pressure of CO_2 in the atmosphere and its calculated concentration in the water. Instead of using monthly time steps, an adjustment to a higher temporal resolution, leading to a more frequent exchange with the atmosphere, could potentially increase the amount of outgassed carbon.

For assessing the effects of climate change on riverine carbon and exported carbon pools and fluxes, we calculated their relative differences. Although the absolute simulated amounts and concentrations may not completely fit the observations, we are sure that the relative changes still provide insights into potential future changes.

The riverine carbon pools and fluxes in this tightly coupled system may change during the 21st century in several ways. According to our results climate change will induce a basin-wide increase in riverine carbon pools. Areas most affected are the central and western basin. Here the outgassing of CO_2 , as well as the organic and inorganic carbon pools, increases most clearly.

Our results indicate that projected climate change may alter outgassed carbon (CO_2 evasion) by several means. Firstly, a higher production of terrestrial material leads to an increase in organic carbon available for respiration; secondly, the higher atmospheric CO_2 concentration leads to an in-

crease in dissolved inorganic carbon in the water. Thirdly, higher water temperatures decrease the solubility of CO_2 in the water but also increase the respiration rates. Overall, a combination of these factors may lead to a considerable increase in CO_2 evasion and a slight increase in exported riverine carbon. Spatially, the results are heterogeneous. The amount of outgassed carbon increases in most parts of the basin. This pattern is mainly driven by the increased amount of organic carbon available for respiration. However, even in areas where organic carbon does not increase, or even decreases, the amount of outgassed carbon is elevated. This is mainly caused by the increased respiration rate at higher temperatures. Thus, even with less carbon available, higher temperatures lead to an elevated outgassing of CO_2 . As a consequence of an increased evasion of CO_2 , an additional increase in atmospheric CO_2 concentration can occur. However, the simulated amount of outgassed carbon under current conditions is underestimated in comparison to observations by a factor of up to one sixth. The observations are based on a combination of small-scale measurements of CO_2 evasion and remotely sensed estimates of inundated area (Belger et al., 2011; Moreira-Turcq et al., 2003; Richey et al., 1990, 2002). In contrast, the outgassing calculated in RivCM is a more aggregated estimate. In reality during the rising-water stage, small changes in discharge can lead to a comparably larger non-linear increase in inundated area. This is not taken into account in RivCM. In RivCM the outgassing depends only on the inorganic carbon concentration in the water and the partial pressure of CO_2 . Additionally to the inundated area, the vegetation coverage also affects the outgassing of CO_2 from flooded area as Abril et al. (2014) show. Including the production of allochthonous organic material, which is not included in RivCM, may also change the amount of outgassed carbon. But in contrast to the other processes the production via photosynthesis may lead to an increase in the CO_2 evaded to the atmosphere. Furthermore, including the evasion of CO_2 from inundated soils, which represents a process that may lead to a further increase in simulated CO_2 outgassing, in RivCM would help to simulate outgassing that is more in agreement with observation-based estimates.

Besides riverine carbon fluxes such as outgassed carbon, climate change also affects riverine carbon pools. However, these changes are not homogeneously distributed across the basin. The increase in organic carbon (POC and DOC) is on the one hand caused by the change in inundation patterns. This can be seen mainly in the western part of the basin, resulting from a projected increase in precipitation, particularly in the SRES-A2 scenario (Langerwisch et al., 2013). On the other hand, more rainfall and increased atmospheric CO_2 concentration may lead to increased amounts of available organic carbon, i.e. more biomass under future climate conditions (e.g. Huntingford et al., 2013), which may directly increase the POC and DOC pools. As a consequence of the additional riverine organic carbon, a depletion of oxygen caused by enhanced respiration in the water can occur

(Junk and Wantzen, 2004; Melack and Fisher, 1983). The resulting anoxia can lead, for example, to denitrification or the production of methane (Lampert and Sommer, 1999). In areas with already reduced O_2 levels, such as flooded forests during falling water, the further depletion of oxygen can potentially affect fish and other animal groups inhabiting the water (Hamilton et al., 1997; Melack and Fisher, 1983). The comparison with measured data (Cole and Caraco, 2001; Ertel et al., 1986; Hedges et al., 1994; Moreira-Turcq et al., 2003; Neu et al., 2011) shows that the concentrations of the different simulated carbon pools fit in the range of observations, with only a slight overestimation for POC. These results also show that the inclusion of allochthonous organic material is not necessarily needed to reproduce the observed POC concentrations in the water. The agreement of simulated with observed POC, DOC and IC concentrations shows the reliability of RivCM because the errors in concentration measurements are small.

The amount of riverine inorganic carbon which remains in the water and does not evade to the atmosphere is projected to increase under climate change. Here, the lower solubility resulting from higher temperatures is not able to balance the effect of a higher atmospheric CO_2 concentration resulting in more dissolved CO_2 . This pattern is consistent within the emission scenarios and the climate models and can be found in most parts of the basin. The 2- to 3-fold increase in inorganic carbon in the water may have serious consequences for fish and fungi, since dissolved inorganic carbon directly lowers the pH in the water (Lampert and Sommer, 1999). In combination with the oxygen depletion discussed above this may severely affect riverine fauna.

4.2 Riverine outgassing and export to the Atlantic Ocean

Our results indicate that climate change alters the proportion of carbon evaded from the river to carbon exported to the ocean. Climate change increases the outgassing of CO_2 with a higher rate than it increases the discharge of organic carbon.

During the reference period, the outgassed carbon from water bodies contributes on average about 3.6 % of all evaded carbon from the entire Amazon basin. This seems to be only a small amount, but in river-dominated regions, this fraction may represent up to 10–50 % of total evaded carbon, which is especially obvious in the eastern part of the basin. The basin-wide proportion of riverine vs. total carbon evasion (including riverine outgassing and CO_2 release during autotrophic and heterotrophic respiration) increases from 3.6 up to 4.3 % from the reference to the future period, which indicates the increasing contribution of riverine outgassed carbon to the total outgassed carbon. Our results show that 3.5 % of the carbon accumulated in terrestrial NPP is released to the atmosphere by outgassing from the river. It can be expected that climate change will alter this fraction to up to 4.2 %, which is due to a combination of increased NPP

and increased CO₂ partial pressure. Inland waters receive about 19×10^{14} g C yr⁻¹ from the terrestrial landscape, of which about 8×10^{14} g C yr⁻¹ are returned to the atmosphere (Cole et al., 2007). Globally the riverine input from land to ocean of organic carbon is estimated to be between 4.5 and 9.0×10^{14} g C yr⁻¹, which is at least the same amount of carbon that is taken up by the oceans from the atmosphere (Bauer et al., 2013; Cole et al., 2007).

The annual export of about 6300 km³ of freshwater from the Amazon River to the Atlantic Ocean (Gaillardet et al., 1997) is accompanied by 40×10^{12} g of organic carbon, which represents 8–10 % of the global organic carbon transported to oceans by rivers (Moreira-Turcq et al., 2003; Richey et al., 1990). Our estimates of the discharge of organic carbon to the Atlantic are larger. As already shown in other studies (Gerten et al., 2004; Langerwisch et al., 2013) LPJmL is able to reproduce observed discharge patterns. As already discussed (Sect. 4.1.) small deviations between observed and simulated discharge or even a small shift in seasonality (1–2 months) can lead to a comparably large difference in discharged carbon because the combination of the simulated concentration and amount of water discharged determines the amount of discharged carbon to the Atlantic Ocean. In addition to this, the overestimation of export to the ocean is partly caused by up- and downscaling of observation data. Our estimates of riverine TOC export represent about 1–2 % of the net basin primary production (Moreira-Turcq et al., 2003), which is in agreement with the results of our study (1 % during reference period). Our results suggest that this proportion will change by –10 to +10 % due to climate change. The continuous input of organic matter into the ocean fundamentally impacts the primary production of the Atlantic Ocean off the coast of South America (Körtzinger, 2003; Cooley and Yager, 2006; Cooley et al., 2007; Subramaniam et al., 2008). In addition to organic carbon, nutrients, which are only marginally taken up by the low primary production within the river, are also exported to the ocean, fuelling oceanic heterotrophy and primary production.

The inclusion of inundation and the corresponding transport and conversion of organic material leads to an increase in outgassed carbon of more than 3 %, which equals about 14.5×10^{12} g month⁻¹. This amount increases to up to 18.3×10^{12} g month⁻¹ due to climate change. The proportion of outgassed carbon from water bodies is an indicator for the importance of the riverine system to the carbon dynamics of the entire basin. It emphasizes the importance of the implementation of floodplain systems to vegetation models, especially for Amazonia. Including inundation and the export of organic material to vegetation models seems to be of minor importance because the carbon is only transported but its quantity does not change. This is only partly true since the organic material is no longer available on site (e.g. as fertilizer) but is removed from one location and finally from the entire system. Including this export leads to a more realistic estimation of carbon fluxes, and ignoring this constant drain

of carbon from the Amazon basin would therefore overestimate the general ability of Amazonia to sequester carbon. Only coupled models can cover the interconnection between land and river, which may be important to identify non-linear feedbacks on climate change (Bauer et al., 2013). Our approach serves as a basis for simulating carbon modification and transport from the terrestrial biosphere through river systems to the oceans and establishes the link between continental and oceanic systems on a continental scale.

5 Summary

We aimed to develop a coupled terrestrial–riverine model to understand the effects of climate change on carbon fluxes in such a coupled system. We applied the model to the Amazon basin which could serve as a blueprint for studying other systems where such a tight coupling of the terrestrial and riverine part appears. With our approach we were able to estimate potential changes in exported and riverine carbon pools and fluxes from present until 2100 for the Amazon basin. We showed that the export of carbon to the Atlantic Ocean could increase slightly by about 1 %, while the export to the atmosphere could increase by about 40 %. To estimate these changes we coupled the newly developed riverine carbon model RivCM to the well-established vegetation and hydrology model LPJmL. These large export fluxes are accompanied with changes in terrestrial organic carbon and riverine organic and inorganic carbon. Our results suggest that coupling terrestrial with riverine carbon is an important step towards a better understanding of the effects of climate change on large-scale catchment carbon dynamics.

The Supplement related to this article is available online at doi:10.5194/esd-7-559-2016-supplement.

Author contributions. Model development: F. Langerwisch, B. Tietjen and W. Cramer. Data analysis: F. Langerwisch, A. Rammig and K. Thonicke. Writing the article: F. Langerwisch, A. Rammig, A. Walz, B. Tietjen and K. Thonicke.

Acknowledgements. We thank the “Pakt für Forschung der Leibniz-Gemeinschaft” for funding the TRACES project for F. Langerwisch. A. Rammig was funded by FP7 AMAZALERT (ProjectID 282664) and Helmholtz Alliance “Remote Sensing and Earth System Dynamics”. We also thank Susanne Rolinski and Dieter Gerten for discussing the hydrological aspects. We thank Alice Boit for fruitful comments on the manuscript. Additionally, we thank our LPJmL and ECOSTAB colleagues at PIK for fruitful comments on the design of the study and the manuscript. We also thank the anonymous reviewers whose comments and suggestions greatly improved the manuscript.

Edited by: R. Aalto

References

- Abril, G., Martinez, J.-M., Artigas, L. F., Moreira-Turcq, P., Benedetti, M. F., Vidal, L., Meziane, T., Kim, J.-H., Bernardes, M. C., Savoye, N., Deborde, J., Souza, E. L., Albéric, P., Landim de Souza, M. F., and Roland, F.: Amazon River carbon dioxide outgassing fuelled by wetlands, *Nature*, 505, 395–398, doi:10.1038/nature12797, 2014.
- Allison, M. A., Nittrouer, C. A., and Kineke, G. C.: Seasonal sediment storage on mudflats adjacent to the Amazon river, *Mar. Geol.*, 125, 303–328, 1995.
- Amon, R. M. W. and Benner, R.: Photochemical and microbial consumption of dissolved organic carbon and dissolved oxygen in the Amazon River system, *Geochim. Cosmochim. Acta*, 60, 1783–1792, 1996.
- Anderson, J. T., Nuttle, T., Saldaña Rojas, J. S., Pendergast, T. H., and Flecker, A. S.: Extremely long-distance seed dispersal by an overfished Amazonian frugivore, *Proc. R. Soc. B Biol. Sci.*, 278, 3329–3335, doi:10.1098/rspb.2011.0155, 2011.
- Aufdenkampe, A. K., Mayorga, E., Hedges, J. I., Llerena, C., Quay, P. D., Gudeman, J., Krusche, A. V., and Richey, J. E.: Organic matter in the Peruvian headwaters of the Amazon: Compositional evolution from the Andes to the lowland Amazon mainstem, *Org. Geochem.*, 38, 337–364, doi:10.1016/j.orggeochem.2006.06.003, 2007.
- Bauer, D. F.: Constructing confidence sets using rank statistics, *J. Am. Stat. Assoc.*, 67, 687–690, 1972.
- Bauer, J. E., Cai, W.-J., Raymond, P. A., Bianchi, T. S., Hopkinson, C. S., and Regnier, P. A. G.: The changing carbon cycle of the coastal ocean, *Nature*, 504, 61–70, doi:10.1038/nature12857, 2013.
- Belger, L., Forsberg, B. R., and Melack, J. M.: Carbon dioxide and methane emissions from interfluvial wetlands in the upper Negro River basin, Brazil, *Biogeochemistry*, 105, 171–183, doi:10.1007/s10533-010-9536-0, 2011.
- Benner, R., Opsahl, S., Chin-Leo, G., Richey, J. E., and Forsberg, B. R.: Bacterial carbon metabolism in the Amazon River system, *Limnol. Oceanogr.*, 40, 1262–1270, 1995.
- Biemans, H., Hutjes, R. W. A., Kabat, P., Strengers, B. J., Gerten, D., and Rost, S.: Effects of precipitation uncertainty on discharge calculations for main river basins, *J. Hydrometeorol.*, 10, 1011–1025, doi:10.1175/2008jhm1067.1, 2009.
- Bogan, T., Mohseni, O., and Stefan, H. G.: Stream temperature-equilibrium temperature relationship, *Water Resour. Res.*, 39, 1245, doi:10.1029/2003wr002034, 2003.
- Bondeau, A., Smith, P. C., Zaehle, S., Schaphoff, S., Lucht, W., Cramer, W., Gerten, D., Lotze-Campen, H., Müller, C., Reichstein, M., and Smith, B.: Modelling the role of agriculture for the 20th century global terrestrial carbon balance, *Global Change Biol.*, 13, 679–706, doi:10.1111/j.1365-2486.2006.01305.x, 2007.
- Bustillo, V., Victoria, R. L., de Moura, J. M. S., Victoria, D. D., Andrade Toledo, A. M., and Colicchio, E.: Biogeochemistry of carbon in the Amazonian floodplains over a 2000-km reach: Insights from a process-Based model, *Earth Interact.*, 15, 1–29, doi:10.1175/2010EI338.1, 2011.
- Coe, M. T., Latrubesse, E. M., Ferreira, M. E., and Amsler, M. L.: The effects of deforestation and climate variability on the streamflow of the Araguaia River, Brazil, *Biogeochemistry*, 105, 119–131, doi:10.1007/s10533-011-9582-2, 2011.
- Cole, J. J. and Caraco, N. F.: Carbon in catchments: connecting terrestrial carbon losses with aquatic metabolism, *Mar. Freshw. Res.*, 52, 101–110, 2001.
- Cole, J. J., Pace, M. L., Carpenter, S. R., and Kitchell, J. F.: Persistence of net heterotrophy in lakes during nutrient addition and food web manipulations, *Limnol. Oceanogr.*, 45, 1718–1730, 2000.
- Cole, J. J., Prairie, Y. T., Caraco, N. F., McDowell, W. H., Tranvik, L. J., Striegl, R. G., Duarte, C. M., Kortelainen, P., Downing, J. A., Middelburg, J. J., and Melack, J.: Plumbing the global carbon cycle: Integrating inland waters into the terrestrial carbon budget, *Ecosystems*, 10, 171–184, doi:10.1007/s10021-006-9013-8, 2007.
- Collatz, G. J., Ribas-Carbo, M., and Berry, J. A.: Coupled photosynthesis-stomatal conductance model for leaves of C4 plants, *Funct. Plant Biol.*, 19, 519–538, doi:10.1071/PP9920519, 1992.
- Cooley, S. R. and Yager, P. L.: Physical and biological contributions to the western tropical North Atlantic Ocean carbon sink formed by the Amazon River plume, *J. Geophys. Res.-Oceans*, 111, C08018, doi:10.1029/2005JC002954, 2006.
- Cooley, S. R., Coles, V. J., Subramaniam, A., and Yager, P. L.: Seasonal variations in the Amazon plume-related atmospheric carbon sink, *Global Biogeochem. Cy.*, 21, GB3014, doi:10.1029/2006GB002831, 2007.
- Cramer, W., Bondeau, A., Woodward, F. I., Prentice, I. C., Betts, R. A., Brovkin, V., Cox, P. M., Fisher, V., Foley, J. A., Friend, A. D., Kucharik, C., Lomas, M. R., Ramankutty, N., Sitch, S., Smith, B., White, A., and Young-Molling, C.: Global response of terrestrial ecosystem structure and function to CO₂ and climate change: results from six dynamic global vegetation models, *Global Change Biol.*, 7, 357–373, 2001.
- Devol, A. H., Quay, P. D., Richey, J. E., and Martinelli, L. A.: The role of gas-exchange in the inorganic carbon, oxygen, and N-222 budgets of the Amazon river, *Limnol. Oceanogr.*, 32, 235–248, 1987.
- Devol, A. H., Forsberg, B. R., Richey, J. E., and Pimentel, T. P.: Seasonal variation in chemical distributions in the Amazon (Solimões) river: A multiyear time series, *Global Biogeochem. Cy.*, 9, 307–328, 1995.
- Diegues, A. C. S.: An inventory of Brazilian wetlands, Union Internationale pour la Conservation de la Nature et de ses Ressources, Switzerland, Gland, Switzerland, 1994.
- Druffel, E. R. M., Bauer, J. E., and Griffin, S.: Input of particulate organic and dissolved inorganic carbon from the Amazon to the Atlantic Ocean, *Geochim. Geophys. Geosyst.*, 6, Q03009, doi:10.1029/2004GC000842, 2005.
- Ertel, J. R., Hedges, J. I., Devol, A. H., Richey, J. E., and Ribeiro, M. D. G.: Dissolved humic substances of the Amazon river system, *Limnol. Oceanogr.*, 31, 739–754, 1986.
- Fader, M., Rost, S., Müller, C., Bondeau, A., and Gerten, D.: Virtual water content of temperate cereals and maize: Present and potential future patterns, *J. Hydrol.*, 384, 218–231, doi:10.1016/j.jhydrol.2009.12.011, 2010.

- Farquhar, G. D., van Caemmerer, S., and Berry, J. A.: A biochemical model of photosynthetic CO₂ assimilation in leaves of C3 species, *Planta*, 149, 78–90, 1980.
- Fearnside, P. M.: Are climate change impacts already affecting tropical forest biomass?, *Global Environ. Change-Hum. Policy Dimens.*, 14, 299–302, doi:10.1016/j.gloenvcha.2004.02.001, 2004.
- Furch, K. and Junk, W. J.: The chemical composition, food value, and decomposition of herbaceous plants, leaves, and leaf litter of floodplain forests, in *The Central Amazon Floodplain*, edited by: Junk, W. J., 187–205, Springer, Berlin, Germany, 1997.
- Gaillardet, J., Dupré, B., Allègre, C. J., and Négrel, P.: Chemical and physical denudation in the Amazon River basin, *Chem. Geol.*, 142, 141–173, 1997.
- Gerten, D., Schaphoff, S., Haberlandt, U., Lucht, W., and Sitch, S.: Terrestrial vegetation and water balance - hydrological evaluation of a dynamic global vegetation model, *J. Hydrol.*, 286, 249–270, doi:10.1016/j.jhydrol.2003.09.029, 2004.
- Gerten, D., Rost, S., von Bloh, W., and Lucht, W.: Causes of change in 20th century global river discharge, *Geophys. Res. Lett.*, 35, L20405 doi:10.1029/2008gl035258, 2008.
- Gordon, W. S., Famiglietti, J. S., Fowler, N. L., Kittel, T. G. F., and Hibbard, K. A.: Validation of simulated runoff from six terrestrial ecosystem models: results from VEMAP, *Ecol. Appl.*, 14, 527–545, doi:10.1890/02-5287, 2004.
- Goulding, M., Barthelm, R., and Ferreira, E.: *The Smithsonian Atlas of the Amazon*, Smithsonian, Washington and London, 2003.
- Gumpenberger, M., Vohland, K., Heyder, U., Poulter, B., Macey, K., Rammig, A., Popp, A., and Cramer, W.: Predicting pan-tropical climate change induced forest stock gains and losses – implications for REDD, *Environ. Res. Lett.*, 5, 14013, doi:10.1088/1748-9326/5/1/014013, 2010.
- Hamilton, S. K., Sippel, S. J., Calheiros, D. F., and Melack, J. M.: An anoxic event and other biogeochemical effects of the Pantanal wetland on the Paraguay River, *Limnol. Oceanogr.*, 42, 257–272, 1997.
- Hedges, J. I., Cowie, G. L., Richey, J. E., Quay, P. D., Benner, R., Strom, M., and Forsberg, B. R.: Origins and processing of organic matter in the Amazon river as indicated by carbohydrates and amino acids, *Limnol. Oceanogr.*, 39, 743–761, 1994.
- Hedges, J. I., Mayorga, E., Tsamakis, E., McClain, M. E., Aufdenkampe, A., Quay, P., Richey, J. E., Benner, R., Opsahl, S., Black, B., Pimentel, T., Quintanilla, J., and Maurice, L.: Organic matter in Bolivian tributaries of the Amazon River: A comparison to the lower mainstream, *Limnol. Oceanogr.*, 45, 1449–1466, 2000.
- Horn, M. H., Correa, S. B., Parolin, P., Pollux, B. J. A., Anderson, J. T., Lucas, C., Widmann, P., Tjiu, A., Galetti, M., and Goulding, M.: Seed dispersal by fishes in tropical and temperate fresh waters: The growing evidence, *Acta Oecologica*, 37, 561–577, doi:10.1016/j.actao.2011.06.004, 2011.
- Huntingford, C., Zelazowski, P., Galbraith, D., Mercado, L. M., Sitch, S., Fisher, R., Lomas, M., Walker, A. P., Jones, C. D., Booth, B. B. B., Malhi, Y., Hemming, D., Kay, G., Good, P., Lewis, S. L., Phillips, O. L., Atkin, O. K., Lloyd, J., Gloor, E., Zaragoza-Castells, J., Meir, P., Betts, R., Harris, P. P., Nobre, C., Marengo, J., and Cox, P. M.: Simulated resilience of tropical rainforests to CO₂-induced climate change, *Nat. Geosci.*, 6, 268–273, doi:10.1038/ngeo1741, 2013.
- Irion, G.: Die Entwicklung des zentral- und oberamazonischen Tieflands im Spät-Pleistozön und im Holozän, *Amazoniana*, 6, 67–79, 1976.
- Irmiler, U.: Litterfall and nitrogen turnover in an Amazonian black-water inundation forest, *Plant Soil*, 67, 355–358, 1982.
- Johnson, M. S., Lehmann, J., Selva, E. C., Abdo, M., Riha, S., and Couto, E. G.: Organic carbon fluxes within and streamwater exports from headwater catchments in the southern Amazon, *Hydrol. Process.*, 20, 2599–2614, 2006.
- Junk, W. J.: The Amazon floodplain – A sink or source for organic carbon?, *Mitteilungen Geol.-Paläontol. Inst. Univ. Hambg.*, 58, 267–283, 1985.
- Junk, W. J. and Piedade, M. T. F.: Plant life in the floodplain with special reference to herbaceous plants, in *The Central Amazon Floodplain*, edited by: Junk, W. J., 147–185, Springer, Berlin, Germany, 1997.
- Junk, W. J. and Wantzen, K. M.: The flood pulse concept: New aspects, approaches and applications - An update, in *Proceedings of the Second International Symposium on the Management of large Rivers for Fisheries*, edited by: Welcomme, R. L. and Petr, T., 117–140, 2004.
- Jupp, T. E., Cox, P. M., Rammig, A., Thonicke, K., Lucht, W., and Cramer, W.: Development of probability density functions for future South American rainfall, *New Phytol.*, 187, 682–693, doi:10.1111/j.1469-8137.2010.03368.x, 2010.
- Keeling, C. D. and Whorf, T. P.: Atmospheric CO₂ records from sites in the SIO air sampling network, in *Trends. A Compendium of Data on Global Change*, Carbon Dioxide Inf. Anal. Cent., Oak Ridge Natl. Lab., US Dep. of Energy, Oak Ridge, Tenn., available at: <http://cdiac.ornl.gov/trends/co2/sio-keel.html> (last access: 11 October 2008), 2003.
- Körtzinger, A.: A significant CO₂ sink in the tropical Atlantic Ocean associated with the Amazon River plume, *Geophys. Res. Lett.*, 30, 2287, doi:10.1029/2003GL018841, 2003.
- Lampert, W. and Sommer, U.: *Limnoökologie*, 2. neu bearbeitete Auflage, Thieme, Stuttgart, 1999.
- Langerwisch, F., Rost, S., Gerten, D., Poulter, B., Rammig, A., and Cramer, W.: Potential effects of climate change on inundation patterns in the Amazon Basin, *Hydrol. Earth Syst. Sci.*, 17, 2247–2262, doi:10.5194/hess-17-2247-2013, 2013.
- Lauerwald, R., Laruelle, G. G., Hartmann, J., Ciaï, P., and Regnier, P. A. G.: Spatial patterns in CO₂ evasion from the global river network, *Global Biogeochem. Cy.*, 29, 534–554, doi:10.1002/2014GB004941, 2015.
- Lehner, B. and Döll, P.: Development and validation of a global database of lakes, reservoirs and wetlands, *J. Hydrol.*, 296, 1–22, doi:10.1016/j.jhydrol.2004.03.028, 2004.
- Lewin-Koh, N. J. and Bivand, R.: *mapproj: Tools for reading and handling spatial objects*, R package version 0.8-7, 2011.
- Lloyd, J. and Taylor, J. A.: On the temperature-dependence of soil respiration, *Funct. Ecol.*, 8, 315–323, 1994.
- Martius, C.: *Decomposition of Wood*, in *The Central Amazon Floodplain*, edited by: Junk, W. J., 267–276, Springer, Berlin, Germany, 1997.
- Mayorga, E., Aufdenkampe, A. K., Masiello, C. A., Krusche, A. V., Hedges, J. I., Quay, P. D., Richey, J. E., and Brown, T. A.: Young organic matter as a source of carbon dioxide outgassing from Amazonian rivers, *Nature*, 436, 538–541, doi:10.1038/nature03880, 2005.

- McClain, M. E. and Elsenbeer, H.: Terrestrial inputs to Amazon streams and internal biogeochemical processing, in *The Biogeochemistry of the Amazon Basin*, edited by: McClain, M. E., Victoria, R. L., and Richey, J. E., 185–208, Oxford University Press, New York, 2001.
- Meehl, G. A., Stocker, T. F., Collins, W. D., Friedlingstein, P., Gaye, A. T., Gregory, J. M., Kitoh, A., Knutti, R., Murphy, J. M., Noda, A., Raper, S. C. B., Wattersson, I. G., Weaver, A. J., and Zhao, Z.-C.: Global climate projections, in *Climate Change 2007: The Physical Science Basis. Contribution of Working Group I to the Fourth Assessment Report of the Intergovernmental Panel on Climate Change*, edited by: Solomon, S., Qin, D., Manning, M., Chen, Z., Marquis, M., Averyt, K. B., Tignor, M., and Miller, H. L., Cambridge University Press, Cambridge, UK and New York, NY, USA, 2007.
- Melack, J. M. and Fisher, T. R.: Diel oxygen variations and their ecological implications in Amazon floodplain lakes, *Arch. Fier Hydrobiol.*, 98, 422–442, 1983.
- Melack, J. M. and Forsberg, B.: Biogeochemistry of Amazon floodplain lakes and associated wetlands, in: *The Biogeochemistry of the Amazon Basin and its Role in a Changing World*, edited by: McClain, M. E., Victoria, R. L., and Richey, J. E., 235–276, Oxford University Press, 2001.
- Melack, J. M., Hess, L. L., Gastil, M., Forsberg, B. R., Hamilton, S. K., Lima, I. B. T., and Novo, E. M. L.: Regionalization of methane emissions in the Amazon Basin with microwave remote sensing, *Global Change Biol.*, 10, 530–544, doi:10.1111/j.1529-8817.2003.00763.x, 2004.
- Melack, J. M., Novo, E. M. L. M., Forsberg, B. R., Piedade, M. T. F., and L., M.: Floodplain ecosystem processes, in *Amazonia and Global Change*, edited by: Keller, M., Bustamante, M., Gash, J., and Silva Dias, P., 525–541, American Geophysical Union, Washington, DC, 2009.
- Mitchell, T. D. and Jones, P. D.: An improved method of constructing a database of monthly climate observations and associated high-resolution grids, *Int. J. Climatol.*, 25, 693–712, doi:10.1002/joc.1181, 2005.
- Moreira-Turcq, P., Seyler, P., Guyot, J. L., and Etcheber, H.: Exportation of organic carbon from the Amazon River and its main tributaries, *Hydrol. Process.*, 17, 1329–1344, doi:10.1002/hyp.1287, 2003.
- Müller-Hohenstein, K.: Die Tropenzone, in *Die Landschaftsgürtel der Erde*, 51–96, edited by: Teubner, B. G., Stuttgart, 1981.
- Nakićenović, N., Davidson, O., Davis, G., Grübler, A., Kram, T., Lebre La Rovere, E., Metz, B., Morita, T., Pepper, W., Pitcher, H., Sankovski, A., Shukla, P., Swart, R., and Dadi, Z.: IPCC Special report on emission scenarios, available at: <http://www.ipcc.ch/ipccreports/sres/emission/index.php?idp=0>, 2000.
- Nepstad, D. C., Tohver, I. M., Ray, D., Moutinho, P., and Cardinot, G.: Mortality of large trees and lianas following experimental drought in an Amazon forest, *Ecology*, 88, 2259–2269, doi:10.1890/06-1046.1, 2007.
- Neu, V., Neill, C., and Krusche, A. V.: Gaseous and fluvial carbon export from an Amazon forest watershed, *Biogeochemistry*, 105, 133–147, doi:10.1007/s10533-011-9581-3, 2011.
- Oksanen, J., Blanchet, F. G., Kindt, R., Legendre, P., O'Hara, R. B., Simpson, G. L., Solymos, P., Stevens, M. H. H., and Wagner, H.: *vegan: Community Ecology Package*, R package version 1.17.11, available at: <http://CRAN.R-project.org/package=vegan>, 2011.
- Österle, H., Gerstengarbe, F. W., and Werner, P. C.: Homogenisierung und Aktualisierung des Klimadatensatzes des Climate Research Unit der Universität of East Anglia, Norwich. 6. Deutsche Klimatagung 2003 Potsdam, Germany, Terra Nostra, 6, 326–329, 2003.
- Panday, P. K., Coe, M. T., Macedo, M. N., Lefebvre, P., and Castanho, A. D. de A.: Deforestation offsets water balance changes due to climate variability in the Xingu River in eastern Amazonia, *J. Hydrol.*, 523, 822–829, doi:10.1016/j.jhydrol.2015.02.018, 2015.
- Parker, A. J.: The Topographic Relative Moisture Index: An approach to soil-moisture assessment in mountain terrain, *Phys. Geogr.*, 3, 160–168, 1982.
- Poulter, B., Aragão, L., Heyder, U., Gumpenberger, M., Heinke, J., Langerwisch, F., Rammig, A., Thonicke, K., and Cramer, W.: Net biome production of the Amazon Basin in the 21st century, *Global Change Biol.*, 16, 2062–2075, doi:10.1111/j.1365-2486.2009.02064.x, 2009a.
- Poulter, B., Aragão, L., Heyder, U., Gumpenberger, M., Heinke, J., Langerwisch, F., Rammig, A., Thonicke, K., and Cramer, W.: Net biome production of the Amazon Basin in the 21st century, *Global Change Biol.*, 16, 2062–2075, doi:10.1111/j.1365-2486.2009.02064.x, 2009b.
- R Development Core Team and contributors worldwide, N. J.: *stats: The R Stats Package version 2.13.0.*, 2011.
- Rammig, A., Jupp, T., Thonicke, K., Tietjen, B., Heinke, J., Ostberg, S., Lucht, W., Cramer, W., and Cox, P.: Estimating the risk of Amazonian forest dieback, *New Phytol.*, 187, 694–706, doi:10.1111/j.1469-8137.2010.03318.x, 2010.
- Randall, D. A., Wood, R. A., Bony, S., Colman, R., Fichet, T., Fyfe, J., Kattsov, V., Pitman, A., Shukla, J., Srinivasan, J., Stouffer, R. J., Sumi, A., and Taylor, K. E.: Climate models and their evaluation, in *Climate Change 2007: The Physical Science Basis. Contribution of Working Group I to the Fourth Assessment Report of the Intergovernmental Panel on Climate Change*, edited by: Solomon, S., Qin, D., Manning, M., Chen, Z., Marquis, M., Averyt, K. B., Tignor, M., and Miller, H. L., Cambridge University Press, 589–662, 2007.
- Richey, J. E. and Victoria, R. L.: C, N, and P export dynamics in the Amazon river, in *Interactions of C, N, P and S Biogeochemical Cycles and Global Change*, vol. Vol. 14, Springer Berlin Heidelberg, Berlin, Heidelberg, available at: <http://nbn-resolving.de/urn:nbn:de:1111-201111152598> (last access: 4 April 2014), 1993.
- Richey, J. E., Hedges, J. I., Devol, A. H., Quay, P. D., Victoria, R., Martinelli, L., and Forsberg, B. R.: Biogeochemistry of carbon in the Amazon River, *Limnol. Oceanogr.*, 35, 352–371, 1990.
- Richey, J. E., Melack, J. M., Aufdenkampe, A. K., Ballester, V. M., and Hess, L. L.: Outgassing from Amazonian rivers and wetlands as a large tropical source of atmospheric CO₂, *Nature*, 416, 617–620, doi:10.1038/416617a, 2002.
- Rost, S., Gerten, D., Bondeau, A., Lucht, W., Rohwer, J., and Schaphoff, S.: Agricultural green and blue water consumption and its influence on the global water system, *Water Resour. Res.*, 44, W09405 doi:10.1029/2007wr006331, 2008.
- Sander, R.: *Compilation of Henry's law constants for inorganic and organic species of potential importance in environmental chemistry*, Air Chemistry Department, Max-Planck Institute of Chem-

- istry, available at: <http://www.mpch-mainz.mpg.de/~sander/res/henry.html>, 1999.
- Schwoerbel, J. and Brendelberger, H.: Einführung in die Limnologie, 9. Auflage, Elsevier, Spektrum Akademischer Verlag, Heidelberg, 2005.
- Sioli, H.: Sedimentation im Amazonasgebiet, *Int. J. Earth Sci.*, 45, 608–633, 1957.
- Sitch, S., Smith, B., Prentice, I. C., Arneeth, A., Bondeau, A., Cramer, W., Kaplan, J. O., Levis, S., Lucht, W., Sykes, M. T., Thonicke, K., and Venevsky, S.: Evaluation of ecosystem dynamics, plant geography and terrestrial carbon cycling in the LPJ dynamic global vegetation model, *Global Change Biol.*, 9, 161–185, doi:10.1046/j.1365-2486.2003.00569.x, 2003.
- Sjögersten, S., Black, C. R., Evers, S., Hoyos-Santillan, J., Wright, E. L., and Turner, B. L.: Tropical wetlands: A missing link in the global carbon cycle?: Carbon cycling in tropical wetlands, *Global Biogeochem. Cy.*, 28, 1371–1386, doi:10.1002/2014GB004844, 2014.
- Subramaniam, A., Yager, P. L., Carpenter, E. J., Mahaffey, C., Bjorkman, K., Cooley, S., Kustka, A. B., Montoya, J. P., Sanudo-Wilhelmy, S. A., Shipe, R., and Capone, D. G.: Amazon River enhances diazotrophy and carbon sequestration in the tropical North Atlantic Ocean, *P. Natl. Acad. Sci.*, 105, 10460–10465, doi:10.1073/pnas.0710279105, 2008.
- Thonicke, K., Spessa, A., Prentice, I. C., Harrison, S. P., Dong, L., and Carmona-Moreno, C.: The influence of vegetation, fire spread and fire behaviour on biomass burning and trace gas emissions: results from a process-based model, *Biogeosciences*, 7, 1991–2011, doi:10.5194/bg-7-1991-2010, 2010.
- Vannote, R. L., Minshall, G. W., Cummins, K. W., Sedell, J. R., and Cushing, C. E.: River Continuum Concept, *Can. J. Fish. Aquat. Sci.*, 37, 130–137, 1980.
- Wagner, W., Scipal, K., Pathe, C., Gerten, D., Lucht, W., and Rudolf, B.: Evaluation of the agreement between the first global remotely sensed soil moisture data with model and precipitation data, *J. Geophys. Res.*, 108, 4611, doi:10.1029/2003JD003663, 2003.
- Wantzen, K. M., Yule, C. M., Mathooko, J. M., and Pringle, C. M.: Organic matter processing in tropical streams, in *Aquatic Ecosystems: Tropical Stream Ecology*, 43–64, Elsevier Science (USA), London, 2008.
- Waterloo, M. J., Oliveira, S. M., Drucker, D. P., Nobre, A. D., Cuartas, L. A., Hodnett, M. G., Langedijk, I., Jans, W. W. P., Tomasella, J., de Araújo, A. C., Pimentel, T. P., and Estrada, J. C. M.: Export of organic carbon in run-off from an Amazonian rain-forest blackwater catchment, *Hydrol. Process.*, 20, 2581–2597, 2006.
- Worbes, M.: The forest ecosystem of the floodplains, in *The Central Amazon Floodplain*, edited by: Junk, W. J., 223–265, Springer, Berlin, Germany, 1997.
- WWF HydroSHEDS: HydroSHEDS, available at: <http://hydrosheds.cr.usgs.gov/> (last access: 15 October 2007), 2007.
- Yarnell, S. M., Mount, J. F., and Larsen, E. W.: The influence of relative sediment supply on riverine habitat heterogeneity, *Geomorphology*, 80, 310–324, doi:10.1016/j.geomorph.2006.03.005, 2006.
- Zulkafli, Z., Buytaert, W., Manz, B., Rosas, C. V., Willems, P., Lavado-Casimiro, W., Guyot, J.-L., and Santini, W.: Projected increases in the annual flood pulse of the Western Amazon, *Environ. Res. Lett.*, 11, 14013, doi:10.1088/1748-9326/11/1/014013, 2016.